

FACILITY FORM 608	N64-33177	(THRU)
	43	1
	MASACB 59205	3N
	(PAGES)	(CATEGORY)
	(NASA CR OR TMX OR AD NUMBER)	

Technical Report No. 32-410

Protection Requirements for the Resistance of Meteoroid Penetration Damage of Interplanetary Spacecraft Systems

John J. Volkoff

OTS PRICE

XEROX	\$	2.00 FS
MICROFILM	\$.50 MF



JET PROPULSION LABORATORY
CALIFORNIA INSTITUTE OF TECHNOLOGY
PASADENA, CALIFORNIA

July 1, 1964

Copyright © 1964
Jet Propulsion Laboratory
California Institute of Technology

Prepared Under Contract No. NAS 7-100
National Aeronautics & Space Administration

Technical Report No. 32-410

*Protection Requirements for the Resistance of
Meteoroid Penetration Damage of
Interplanetary Spacecraft Systems*

John J. Volkoff


John W. Stearns, Jr., Acting Chief
Advanced Propulsion Engineering

JET PROPULSION LABORATORY
CALIFORNIA INSTITUTE OF TECHNOLOGY
PASADENA, CALIFORNIA

July 1, 1964

CONTENTS

Nomenclature and Terminology	v
I. Introduction	1
II. Nature of Meteoroids	2
A. The Near-Earth Region	4
B. The Interplanetary Region	8
C. The Asteroid Region	9
D. The Planetary Region	11
E. A Meteoroid Model	13
III. Meteoroid-Penetration Resistance Analysis	14
A. The Variable-Flux Environment	15
B. The Variable Flux-Intensity Environment	17
C. The Constant-Flux Environment	18
D. Application of Section IIIB	18
IV. A Meteoroid Flux-Intensity Profile for a Planetary Mission	21
V. Protection Requirement Estimates	29
A. Vulnerable Area	29
B. Heat-Rejection Radiator Mass	29
C. Penetration and Spalling	31
D. Erosion	31
VI. Discussion	32
VII. Conclusion	34
Acknowledgment	34
References	35

FIGURES

1. Actual longitudinal profile of meteoric flux in the ecliptic plane . . .	5
2. Meteoric flux vs ecliptic latitude	5
3. Planet shielding factor S_h vs ratio of effective altitude D to radius of essential planetary meteoric envelope R	6
4. Meteoroid flux intensity vs geocentric distance ratio.	7
5. Observed meteor velocity distribution	7
6. Factor J vs meteoroid velocity for meteoroid-density parameters . . .	20
7. Factor K_8 vs target-material density	20
8. Jupiter orbiter mission plan.	21
9. Spiral-out from Earth trajectory.	21
10. Jupiter orbiter mission trajectory	22
11. Jupiter orbiter flux-intensity profile	23
12. Lunar encounter flux-intensity profile	24
13. Solar probe flux-intensity profile	25
14. Mercury orbiter and flyby flux-intensity profile	25
15. Venus orbiter flux-intensity profile for various circular orbits . . .	26
16. Mars orbiter flux-intensity profile for various circular orbits . . .	26
17. Uranus probe flux-intensity profile.	27
18. Saturn orbiter flux-intensity profile.	27
19. Neptune probe flux-intensity profile	28
20. Pluto probe flux-intensity profile	28
21. 500-kwe nuclear-electric space cruiser	30

TABLES

1. Density distribution of bright meteors	8
2. Planetary data	12
3. Spacecraft heliocentric trajectories	22
4. Spacecraft planetary spiral-in trajectories.	26
5. Summary of protection requirement ratio R for planetary and interplanetary missions	31
6. Results of protection requirement ratio R as a function of model uncertainty	33

NOMENCLATURE

a	major radius of an ellipse, m	t	time, sec
A	vulnerable area, m^2	T	total time, sec
b	minor radius of an ellipse, m	v	meteoroid relative velocity, m/sec
c	meteoroid concentration, particles/ m^3	α	cumulative meteoroid flux-intensity parameter
C	sonic velocity $(g_c E_\tau \rho_\tau^{-1})^{1/2}$, m/sec	β	flux gradient of the cumulative mass distribution
d	projectile diameter, m	γ	empirical parameter
D	altitude to the essential meteoric envelope near the planet's surface, m	Δ	armor thickness, m
E	bulk modulus of elasticity, g/ m^2	ϵ	eccentricity
f	failure rate, sec^{-1}	η	empirical parameter
F	planet's geometrical factor	φ	empirical parameter
g_c	gravitational force; at Earth's surface, it is 9.807 m/ sec^2	λ	angle from the surface normal, deg
G	planetary surface gravitational force normalized to Earth's gravitational force, dimensionless	Φ	cumulative meteoroid flux, number of particles/ m^2 sec
H	hardness property $(g_c H_\tau \rho_\tau^{-1})^{1/2}$, m/sec	ϑ	empirical parameter
H	brinell hardness, g/ m^2	Θ	true anomaly angle, deg
$I(t)$	normalized flux intensity, Eq. (36), dimensionless	μ	gravitational parameter (Ref. 54), m^3/sec^2
J	integrated angle dependency factor, Eq. (30), dimensionless	ρ	meteoroid particle density, g/ m^3
K	constant	ψ	erosion depth, micron
m	meteoric particle mass, g	ω	heliocentric direction of meteoroids, rad
M	material parameter	Subscripts	
P_c	crater depth, m	c	constant or near-Earth
$P_{(n)}$	probability of n impacts	e	Earth
r	space location	p	planet
R	planetocentric distance, m	p	meteoroid particles or projectile
\mathcal{R}	protection requirement ratio for an interplanetary mission relative to that for a near-Earth orbital mission [Eq. (35)], dimensionless	o	reference
S_h	planet shielding factor	s	solar or spatial
		s/c	spacecraft
		τ	target
		v	variable or interplanetary
		z	selected

TERMINOLOGY

Meteoroid. A solid object in interplanetary space whose origin is of cometary, asteroidal, or of secondary meteoritic generation.

Meteor. A meteoroid which enters the atmosphere of a planet and produces light.

Meteorite. A meteoroid which reaches the planet's surface without being completely vaporized.

Meteoric. Of or pertaining to meteoroids located in space whether or not the space includes an atmosphere.

Meteoroidal. Of or pertaining to meteoroids located specifically in interplanetary space.

Cometary. Of or pertaining to comets.

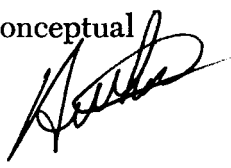
Asteroidal. Of or pertaining to asteroids.

ABSTRACT

33/77

A study of spacecraft component and system protection requirements for the resistance of meteoroid penetration damage is presented for various planetary and interplanetary missions. Meteoroidal characteristics and their distributions in planetary, asteroid belt, and interplanetary space regions are discussed. A meteoroid model derived from this study is applied to typical missions for nuclear-electric spacecraft, and corresponding meteoroid flux-intensity profiles are determined.

A technique to estimate the armor requirement for any interplanetary mission is developed and discussed. The armor requirement for interplanetary missions is compared to that for near-Earth conventional estimates and applied to the radiator systems of a conceptual 500-kwe nuclear-electric spacecraft.



I. INTRODUCTION

Meteoric matter in space is capable of damaging spacecraft systems to the degree of jeopardizing the success of scientific space exploration. Protection requirements to resist meteoroid impact damage are therefore necessary for increased spacecraft reliability during interplanetary or planetary spacecraft missions.

Three sources of information that play a major role in establishing spacecraft system protection requirements for the resistance of meteoroid penetration damage are astronomy, satellite and space-probe research, and hypervelocity-projectile impact studies. The nature, properties, and impact effects of meteoric matter have been postulated from interpreted data obtained from observations, measurements, and theoretical approximations.

To determine the probable meteoric flux that will be encountered by spacecraft in space, the spacecraft trajectory and meteoroid distribution along the trajectory must be known. For most interplanetary spacecraft flights, the trajectory includes spiral-out to escape, heliocentric transfer, and planetary encounter phases. The meteoroid flux distribution can be estimated for planetary, asteroid, and interplanetary regions. From these data, a probable meteoroid flux profile for such trajectories can be constructed.

Since it is not feasible to protect a spacecraft system for a zero probability of meteoroid penetration, the problem confronting the system designer is the tradeoff between system reliability and system mass economics

integrated over the desired operational time. System reliability must be sufficiently high so that the success of scientific missions will not be overly jeopardized, and system mass must be sufficiently low so that an acceptable scientific payload may be delivered.

Protection requirements are a function of many parameters, which include vulnerable area, exposure time to the expected meteoroid flux, desired probability of no penetration damage, meteoroid characteristics, and system material properties. Armor and bumper-shielding techniques are currently the most feasible protection systems. Armor protection, relative to bumper-shielding protection, is generally a more significant item in spacecraft design because of its greater mass contribution to a spacecraft system.

The critical subsystems of a nuclear-electric spacecraft requiring armor-type protection are the heat-rejection radiators, propellant storage tank, control mechanisms, and fluid-transfer lines. Some systems may inherently possess a reasonably high resistance to meteoroid impact damage simply by the nature of their configurations. The boiler, for example, usually contains enough wall material to provide a high degree of resistance to penetration damage. As another example, a star-seeker has by nature a small exposed area and hence requires relatively little protection from the meteoroid environment. In this study, the heat-rejection radiators of the power-generation system, because of their high vulnerability, will serve as a representative component requiring armor-protection consideration.

Armor thickness is often estimated by assuming the meteoroid flux to be that of near-Earth and remaining

constant over the mission lifetime. This concept usually results in massive systems that have unrealistic and intolerable armor requirements for interplanetary missions of present interest.

An investigation of the various regions that may be encountered by an interplanetary spacecraft indicated that the meteoroid flux, density, and impact velocity, vary extensively. In addition, geometrical parameters of a spacecraft component influence the exposure to the expected meteoroid environment. When the variable nature of these parameters is accounted for, a more sophisticated calculational procedure is required to determine realistic protection requirements to resist meteoroid penetration damage. This procedure is developed in this study.

The nature of meteoroids in the various regions traversed during a planetary or interplanetary mission is studied to develop a meteoroid model. A selected meteoroid-penetration resistance criterion is incorporated with the spacecraft trajectory and the meteoroid model to yield an estimated flux-intensity profile for the mission.

The flux-intensity profile is used to evaluate the meteoroid particle mass which corresponds to a specified probability of no penetrating impacts. The minimum meteoroid particle mass associated with this probability can be compared to that for the near-Earth constant-flux region from which a ratio of protection requirement for a specified interplanetary mission to a near-Earth orbital mission can be obtained. This ratio can be used to evaluate the armor protection necessary for the interplanetary mission to meet a specified probability of no meteoroid impact damage.

II. NATURE OF METEOROIDS

The accumulated data from measurements and theoretical analyses reveal that the nature of meteoric matter in space is quite variable and anisotropic. The heliocentric motion is both direct and retrograde. Various perturbation effects influence the direction and distribution of meteoric matter. Regional meteoroid concentrations

and flux vary by orders of magnitude. Geocentric particle velocity varies up to about 80 km/sec. The density of meteoroids ranges from approximately 0.01 to 8 g/cm³. Composition and structural characteristics also vary in a range from hypothetical porous (icy-type) models to stony and metallic solid objects.

In view of this known maze of variable characteristics, it is difficult to assign an average value to each of these meteoroidal parameters for the planetary and interplanetary regions. Complete foreknowledge covering these meteoroidal characteristics may never be attainable because of the uncertain and continuously varying developments of meteoric matter in the extensive spatial environment. Because of the scanty and limited data accumulated from astronomical and satellite and spaceprobe research, an attempt to develop a meteoroid model at this early stage may therefore be considered at best a conjecture. However, average integrated values covering the variable meteoroidal characteristics may be reasonably selected for the purpose of estimating conservative protection requirements necessary to resist meteoroid impact damage to spacecraft systems and components. Before proceeding to describe the proposed meteoroid model for the various regions which are traversed during a planetary or interplanetary mission, it may be well to briefly describe the general nature of meteoric matter in space.

Meteoric matter may be classified as asteroidal or cometary. About 90% of the total meteoric debris accreted by the Earth is associated with present or past comets; the remainder is contributed by asteroidal matter. There seems to be no evidence that comets have an interstellar origin. All appear to be permanent members of the solar system. About half of them move in direct orbits, while the remaining half are in retrograde motion. The majority of the observed comets move in planes tilted at nearly right angles (60 to 130 deg) to the plane of the ecliptic, with very few lying in this plane. The debris having orbits of great inclinations are believed to be long-lived and are less likely to be dispersed due to the smaller probability of being perturbed by the planets. It appears that the majority of near-parabolic comets have perihelion distances that are well within 2 AU. About 43% of the cumulative number of these comets pass inside the Earth's orbit and about 87% pass within 2 AU (Ref. 1). The very few found far from the Sun are believed to be very large comets, and may represent a multitude of comets appearing to be integrated as one comet.

Periodic comets, observed at more than one apparition, move in the same direction as the planets. The majority of such comets have orbital planes tilted at less than 45 deg to that of the Earth's. Only Halley's comet has an orbital inclination exceeding 90 deg. The most common eccentricities of short-period comet orbits are found to be around 0.5. Their perihelion distances predominately

range between 1 and 2 AU, with very few passing within the Earth's orbit (Ref. 1).

The material of a comet is dispersed by a wide variety of operating mechanisms and forces. Continual loss of material into the comet's tail is primarily due to particulate collisions, electrical repulsion produced by photoelectric action of sunlight, and cosmic rays. Existing cohesive forces and gravitational attraction oppose the forces which tend to disperse cometary fragments.

All short-period comets undergo many perturbations and are constantly disintegrating. Their low inclinations keep them near the Earth's orbital plane. As the particles become dispersed, they become thinly spread around their vast orbit, thus increasing the chances for a spacecraft to encounter the particles. Since the majority of periodic comets which can supply meteors stay outside the Earth's orbit, it is assumed that much undiscovered meteoric debris exists in orbits at various inclinations between the planets. However, it seems highly improbable that comets moving in short-period orbits with a high inclination to the ecliptic plane have escaped detection.

Stream and sporadic meteors are believed to be associated with present or past comets. Similar to comets, the orbital inclinations for both stream and sporadic meteors are high and predominately lie within 35 deg. The orbital inclinations tend to increase with increased periods, which indicates that particle concentration increases toward the plane of the ecliptic with decreasing solar distances. It is believed that many meteor showers, such as the Perseids, continue in their same path and gradually become uniformly spread around their entire orbit. Some particles of meteor showers move in parallel paths very close to the comet orbit; others are bunched near the parent comet and represent early stage formation, thereby possessing low particle density.

Large meteor particles, sometimes defined as fireballs, are rare among shower meteors. No meteorite has been identified with any known meteor shower. It is therefore postulated that the particles are sorted according to their sizes, and that only those of comparable size move together. About 15% of examined fireballs are made up of solid particles—the rest of them have a porous structure. The density and distribution of the different types generally vary from one shower to another, though several similarities are evident. No significant difference is apparent in the relative percentage of solid and porous particles in sporadic and shower meteors (Ref. 2).

The number of independent shower orbits of small subvisual particles, observed by radio-echo patterns of activity, is very great. The patterns of meteoric activity were found to be extremely variable, thereby implying that occurrence-prediction of particular meteoric showers may be impossible. It is suggested that meteoric activity may be described as sporadic showers, plus occasional predictable showers of large particles (Ref. 3). A greater percentage of meteoric matter (at least 80%) appears to be of sporadic nature. The probability of encounter is much greater for sporadic matter than for stream meteors because sporadics are more abundant and more widely dispersed in their orbital paths; this study shall therefore be concerned primarily with sporadic meteoric matter.

The origin and stability of meteoric dust particles (approximately 1- to 300-micron size range, Ref. 4) have received much attention through zodiacal light and the F-solar corona experiments. The Poyntning-Robertson effect causes small particles to take on more circular orbits and to gradually spiral into the Sun. This effect becomes increasingly selective for particles of smaller size. The dust debris is observed to move in a direct orbit with the Earth and appears to be concentrated near the plane of the ecliptic, possibly influenced by solar and planetary attraction. Data substantiate the theory that a higher meteoroid concentration exists around the Earth than in free space (Ref. 5, 6). Meteoric matter also tends to concentrate near the ecliptic plane and in the asteroid and planetary regions.

The meteoroid flux at any location in space is the product of the meteoroid concentration c and the velocity v of the particles relative to an object at the specified location. The meteoroid flux Φ for particles with mass equal to and greater than m at any time t and heliocentric direction ω at any location r may be expressed as

$$\begin{aligned}\Phi(t, \omega, r) &= \sum_{i=m}^{\infty} c_i(t, \omega, r) \cdot v_i(t, \omega, r) \\ &= \int_m^{\infty} c(t, \omega, r, m) \cdot v(t, \omega, r, m) dm\end{aligned}\quad (1)$$

This may be rewritten as:

$$\Phi(t, \omega, r) = c_{(\geq m)}(t, \omega, r) \cdot v(t, \omega, r) \quad (2)$$

where $c_{(\geq m)}$ is the integrated volumetric concentration of all particles with mass equal to and greater than m , and v is the mean velocity of the meteoroid particles relative to the specified object.

This flux has been found to have a cumulative mass distribution which may be expressed approximately in terms of the meteoroid particle mass m and including all those particles with mass greater than m , as follows:

$$\Phi(t, \omega, r) = \alpha(t, \omega, r) \cdot m^{-\beta(t, \omega, r, m)} \quad (3)$$

where the flux characteristics $\alpha(t, \omega, r)$ and $\beta(t, \omega, r, m)$ define the flux intensity and flux gradient of the cumulative mass-distribution curve, respectively, at any time t and direction ω . The flux gradient may also be a function of the cumulative mass.

For spacecraft trajectories of interest, four regions of space can be distinguished, each presumed to have distinct characteristics. These regions are the near-Earth, interplanetary, asteroid, and planetary. The meteoroid models for these regions are discussed in the ensuing Sections.

A. The Near-Earth Region

Meteoric matter may be expelled from comets by diffusion effects (Ref. 7) and also generated by dust expulsion from the lunar surface caused by meteoroid impacts (Ref. 8, 9). The Earth's gravitational force may be extensive enough to perturb and accrete this meteoric matter. The Earth may also be primarily responsible for the organization of meteoric matter into heliocentric streams at a solar distance of 1 AU. A number of investigations conclude that direct-moving particles in near-circular heliocentric orbits at near 1 AU distance are relatively abundant (Ref. 10). The meteoric concentration in this belt, having particles heliocentrically orbiting in a toroidal-like region, may be several times greater than the concentration found in interplanetary space. Thus meteoric matter from interplanetary space, as well as the most immediate environs, intercept the Earth, suggesting an envelope of meteoric matter peculiar to the Earth (Ref. 11).

Satellite experiments which measure the flux of very small meteoric particles indicate that these particles are in closed orbits around the Earth, thereby confirming the existence of a meteoric dust cloud. Micrometeoroids in this dust cloud predominately have circular orbits. With increasing particle mass, however, the direction tends toward that of elliptical orbits, which is indicated by observed radiant¹ of visible meteors (Ref. 12). The ex-

¹The point in space from which a meteor appears to originate, or the area in space from which shower meteors appear to diverge.

tent of this cloud has been estimated to range to a cis-lunar distance or about 60 Earth radii (Ref. 8). Other investigators suggest that a translunar extent of about 100 Earth radii may be feasible (Ref. 10, 12). Beyond this is the paucity of meteoric matter in interplanetary space.

In the near vicinity of the Earth, the apparent flux of sporadic meteoric particles in the ecliptic plane is more concentrated at the apex of the Earth's way (heliocentric motion) and at the antihelion point (Ref. 13, 14). This phenomenon is caused by the summation of the meteoroid geocentric velocity with the Earth's heliocentric velocity. The actual longitudinal distribution of flux with respect to the Sun may be obtained by subtracting the Earth's orbital effect from the observed flux. The actual longitudinal polar profile of the flux is shown in Fig. 1 and represents the number of meteor orbits which cross the Earth's orbit at any specific direction. This distribution indicates that meteoroid heliocentric movement is predominately direct. The distribution in latitude from the ecliptic plane in the near-Earth vicinity is shown in Fig. 2, which indicates that sporadic meteoric matter is largely concentrated in the ecliptic plane. A satellite at a near-Earth altitude is most likely to encounter longitudinal and altitudinal flux distributions typified by Fig. 1 and 2.

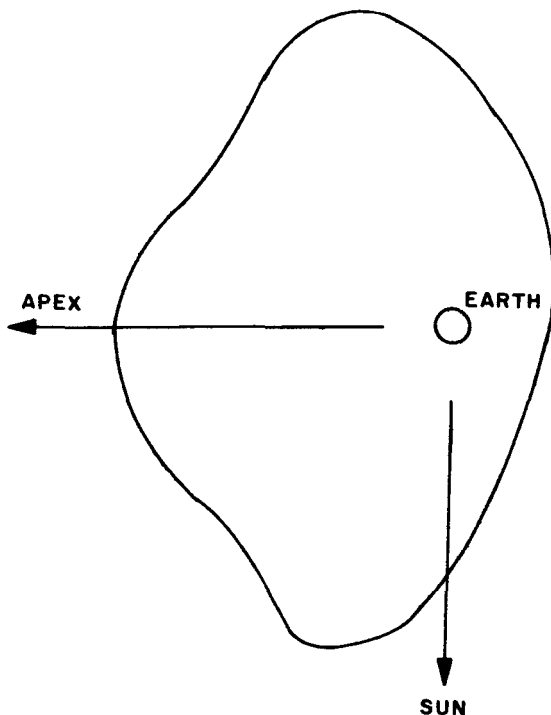


Fig. 1. Actual longitudinal profile of meteoric flux in the ecliptic plane

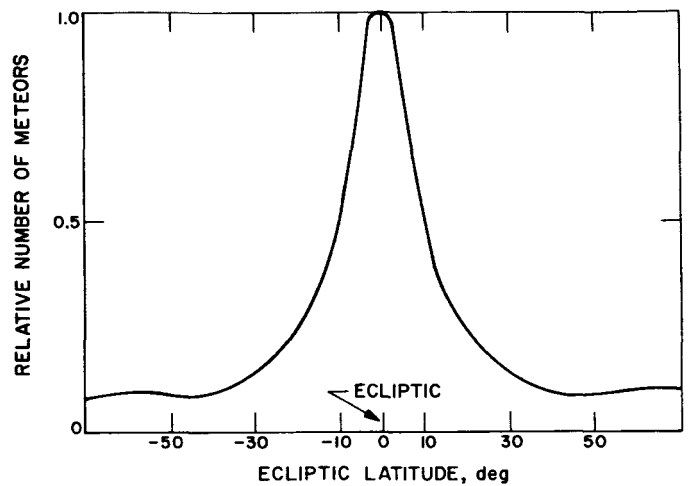


Fig. 2. Meteoric flux vs ecliptic latitude

However, at greater geocentric distances, the effect of shielding heliocentric-orbiting meteoroids by the Earth is decreased, thereby permitting more direct-moving particles to enter the apex region of the Earth's way. Furthermore, particles in heliocentric orbits nearing the Earth, especially those with low relative velocities, are most probably perturbed into parabolic or highly eccentric elliptical orbits about the Earth and are less likely to be visually detected. Very few particles, even those at relatively low velocities, will be perturbed enough by the Earth's gravitational field to be captured into near-circular orbits. The probability of the existence of relatively large particles in nearly circular orbits at very near-Earth altitudes is believed to be very small. The longitudinal flux distribution will, therefore, change from that shown in Fig. 1 to a nearly uniformly distributed flux with increased geocentric distance. The flux distribution will probably become isotropic.

1. Shielding effect

In the near-Earth region, a spacecraft component would probably be impacted by meteoric matter from all directions, if the Earth could be considered transparent. However, this flux must be corrected by the Earth's shielding effect to obtain the actual flux. Assuming the flux direction to be isotropic in space, the shielding factor S_h is given by

$$S_h = \frac{2 - F}{2} \quad (4)$$

where

$$F = \left[\frac{1}{(D/R) + 1} \right]^2 \quad (5)$$

with D the altitude of the essential meteoric envelope near the planet's surface, and R is the planetocentric distance. This is shown in Fig. 3 and is applicable for any planet (Ref. 15).

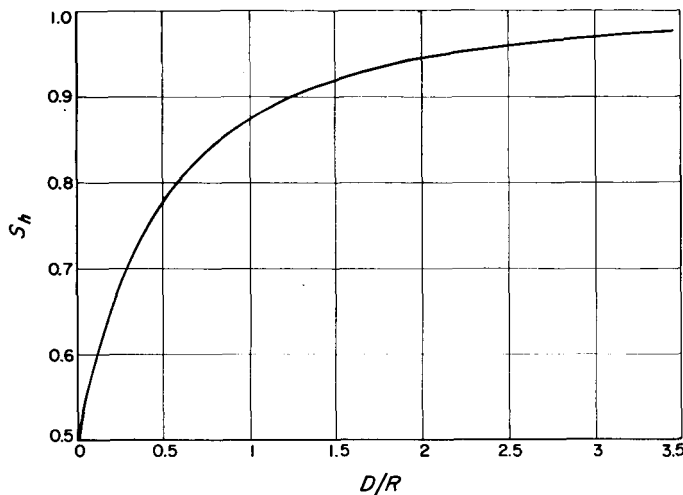


Fig. 3. Planet shielding factor S_h vs ratio of effective altitude D to radius of essential planetary meteoric envelope R

2. Meteoroid flux

The observed meteoroid flux in the near-Earth region is not constant, but has random variations of orders of magnitude (Ref. 16). This is believed due to meteoric showers which may be evident for as long as a few days. Seasonal and diurnal flux variations are also quite significant (Ref. 17, 18).

These random-flux variations above the minimum sporadic threshold may be statistically averaged to derive a reasonable integrated flux if the period of exposure to this environment is relatively large. This integrated flux may be expressed in terms of a cumulative mass distribution [Eq. (3)].

The values for flux-intensity and flux-gradient characteristics in the near-Earth vicinity have been obtained primarily from surveys made by photographic, radio-echo, sounding-rocket, and satellite and space-probe techniques. The α and β terms of Eq. (3) are assumed representative for a randomly oriented surface in space. Utilizing estimated values (Ref. 19) for the terms in Eq. (3), the expression for the average flux at near-Earth distance is

$$\Phi = 7.47 \cdot 10^{-16} \rho_p^{-2.68} m^{-1.34} \quad (6)$$

Equation (6) is not corrected for the Earth's shielding effect. If the mean particle density ρ_p is assumed to be 0.443 g/cc, Eq. (6) becomes

$$\Phi = 6.62 \cdot 10^{-15} m^{-1.34} \quad (7)$$

The flux gradient of small particulate matter measured in the near-Earth vicinity, originating primarily in comets, was found to be different from that estimated by Eq. (6). It is conjectured that solar-radiation pressure may be the dominant factor controlling this difference (Ref. 20). This measured flux, not corrected for Earth's shielding effect, is given by

$$\Phi = 2 \cdot 10^{-17} m^{-1.70} \quad (8)$$

Equation (8) has been proposed for the particle mass range of 10^{-10} to about 10^{-6} g (Ref. 20). Equation (8) is of interest primarily for the study of erosion by micro-meteoroids. The particle mass for which most spacecraft components require reasonable protection from meteoroid penetration damage is generally greater than 0.005 g. Therefore, for this study, Eq. (6) is selected to describe the near-Earth flux.

3. Geocentric flux distribution

The flux intensity of the Earth's accreted matter appears to be distributed inversely as the geocentric distance raised to some power. The value of the exponent suggested by some investigations is likely to be between one and two (Ref. 16, 21). A study of sounding-rocket, space-probe, and satellite data suggests that this power is more likely to be around three (Ref. 22). From zodiacal light calculations (Ref. 8), it appears that there is a tremendous fall-off of flux intensity at low altitudes, becoming less pronounced in the sequence of increasing geocentric distance. Figure 4 shows the flux intensity as a function of geocentric-distance ratios for various estimates of the power. Included are the zodiacal light data.

A calculation shows that the concentration of particles in space around the Earth can be attributed to the Earth's gravitational attraction (Ref. 10). Particles of low velocity relative to Earth, assumed to be abundant at a solar distance of 1 AU, are preferentially attracted to the Earth and possess a relatively higher probability of being captured than higher-velocity particles that similarly come into the Earth's vicinity. It is postulated that a great majority of undetected particles entering the atmosphere have low entering velocities, in the range of 11 to 20 km/sec. The calculations (Ref. 10) show that about 18% of the particles in trajectories approaching within 100 Earth radii are destined to terminate in impacts on the

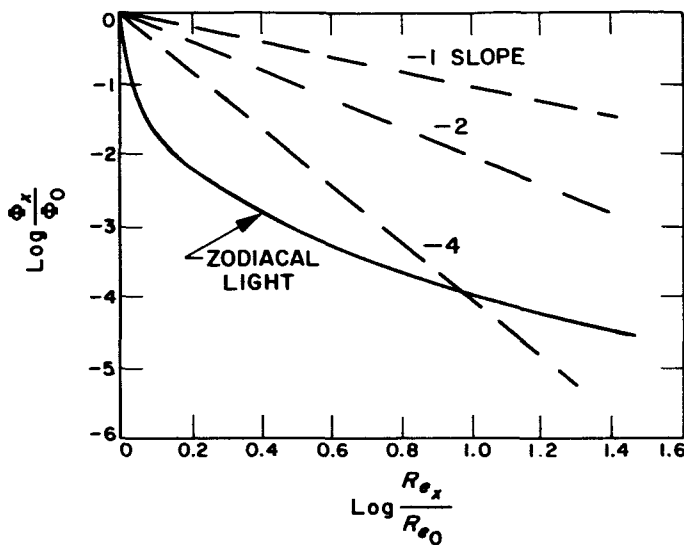


Fig. 4. Meteoroid flux intensity vs geocentric distance ratio

Earth; the remainder may make one or more approaches before returning to heliocentric orbits. None of the particles in the considered trajectories were perturbed into a quasi-permanent orbit. The residence time in the Earth's vicinity was found to range from 5 to 412 days, the median being about 12 days. Of the particles with trajectories approaching within 1800 km of the Earth's surface, about 93% terminate on the Earth.

Particles which pass near the Earth are postulated to have randomly distributed velocity vectors (Ref. 10). Therefore, about the same number of direct meteoroid motions as retrograde motions with respect to the Earth should be found, thus suggesting that the flux in the vicinity of the Earth is essentially isotropic in direction. The geocentric particle velocity is assumed to be a function of distance from the Earth's center and approximately equal to escape velocity. The results of the calculation (Ref. 10) show that steady-state particle concentration near the Earth varies inversely with the 1.15 power of the geocentric distance. The particle flux was found to vary inversely with the 1.66 power of this same distance.

The calculation (Ref. 10) treated the two-body problem with the Earth considered as an isolated body in space. It is also based on a special case of particle trajectory; that is, of direct near-circular heliocentric orbits of low inclination to the ecliptic plane. The results of this calculation have been pointed out to be applicable to a very small percentage of meteoric matter (Ref. 23). Thus, the particle-concentration increase near the Earth attrib-

uted by the Earth's gravitational field may be considerably less than the calculated results indicate.

Another calculation, based on three-body dynamics, shows similar results to those for the two-body one (Ref. 24). Even though these results may not be applicable for all approaching meteoric matter, they nevertheless indicate the general behavior and the order of geocentric distribution of the considered particles under the influence of a gravitational field.

The tenuous upper atmospheric regions may contain a higher accreted concentration of particles affected by atmospheric drag effects. However, because the particle velocity in this region is probably much lower than that of particles above this region, the damaging effects of meteoroid impact on a spacecraft are relatively greatly reduced. Furthermore, the time of exposure in this environment is relatively very small for a realistic spiral-out to escape trajectory. Therefore, for all practical considerations, the hazard of meteoric matter in this zone for interplanetary spacecraft systems is of negligible order.

4. Meteoric particle velocity

Meteor velocities observed by photographic and radio-echo measurements, shown in Fig. 5, indicate a lower limit (comparable to the Earth's escape velocity), and an upper limit (close to the sum of the heliocentric velocity at 1 AU and the Earth's orbital velocity about the Sun, Ref. 25). The observed geocentric velocities indicate that sporadic meteors do not originate from interstellar

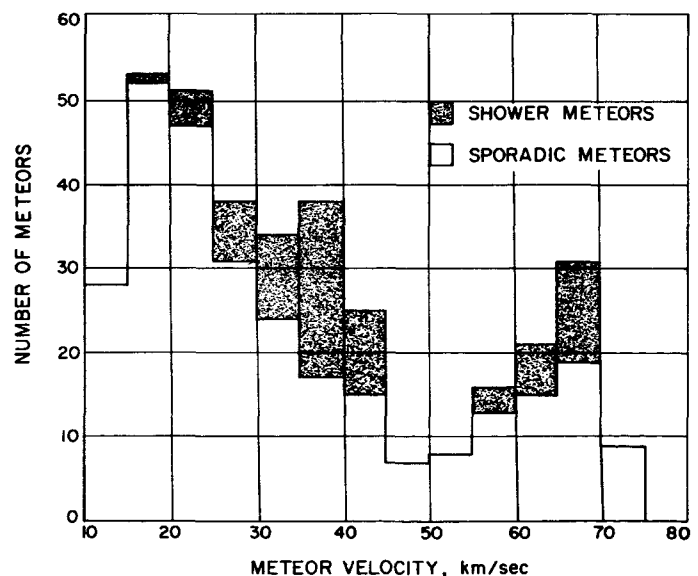


Fig. 5. Observed meteor velocity distribution

space, since their velocities are less than that required for hyperbolic trajectories. It has been shown that only about 0.3% have velocities in the interval of 75 to 79 km/sec. The very few found with velocities greater than 80 km/sec are believed to have been perturbed to these velocities. The typical geocentric velocity distribution of sporadic meteors, presented in Fig. 5, has a double-hump characteristic. This is believed to be attributable to the scarcity of meteors with orbits of small perihelion distances because they are readily removed by solar energy (Ref. 26).

The mean velocity of the sporadic matter at near-atmospheric orbital locations must be slightly higher than the escape velocity, as indicated by Fig. 5. It has been estimated that the mean velocity of meteorites is 16.5 km/sec, and the rms velocity in the Earth's upper atmosphere is estimated to be 17.0 km/sec (Ref. 27). A recent estimate adopts 22.0 km/sec as the mean meteoroid velocity in the near-Earth vicinity (Ref. 19). The velocity profile with respect to geocentric distance is suggested to be closely associated with the Earth escape velocity (Ref. 10).

5. Meteoric particle density

The shape of meteoroid particles has been determined from recoverable rocket experiments. Most of the particles have irregular forms: about a sixth are spherical in form, and the remainder are defined as fluffy.

The distribution with respect to physical structure for sporadic and shower bright meteors has been divided into three fundamental groups: compact bodies, 15%; porous bodies, 48%; and dustballs, 37%. The group density distribution for these bright meteors is shown in Table 1 (Ref. 2). The average density from Table 1 shows a range of 0.49 to 0.79 g/cc. This agrees well with a recent average density estimate of 0.443 g/cc (Ref. 19).

Table 1. Density distribution of bright meteors

Type	Density g/cc	%
Iron	6.6 -7.8	2.19
Stone	3 -4.6	4.38
Light stone	1.3 -2	8.76
Porous bodies	0.5 -0.7	13.86
Porous bodies	0.1 -0.35	34.31
Dustballs	0.01-0.1	34.31
Dustballs	< 0.01	2.19

B. The Interplanetary Region

Meteoric streams, defined as a group of meteoroids in similar orbits, are observed to move in orbits predominantly inclined to the ecliptic plane. Very few are found orbiting very near or in the ecliptic plane. The inclination from the ecliptic plane progressively decreases as the stream groups vary from known streams to spurious streams. Almost all spurious streams and most minor streams cluster principally around the ecliptic plane. This is confirmed by observed elongations of their radiant, which indicate that in the sequence from meteor to meteorite, progressively smaller inclinations to the ecliptic plane are found. However, it is most likely that the inclination distribution of meteoroids in space, and especially near the planets, will have fewer high inclinations than the observed elongations imply, since the probability of observing retrograde encounters is greater than observing direct encounters of a comparable inclination and velocity (Ref. 27).

A spacecraft traversing interplanetary space in the plane of the ecliptic, therefore, is believed to have a very low probability of intercepting a highly concentrated meteoric stream because the intersections of streams with the plane of the ecliptic are nonuniform and widely separated as they sweep across the ecliptic plane (Ref. 28). Furthermore, streams contribute less than 5% of total influx of meteoric matter (Ref. 18). Also, the particle radiant distribution is not as broad as that of minor streams and especially spurious streams (Ref. 29). For example, suppose that a stream possesses a flux 100 times as intense as that of the sporadic flux threshold. This flux intensity is representative of observed meteoric streams (Ref. 30, 31). The flux gradient is assumed to remain unchanged. First, suppose that the probable integrated time exposure in the stream is 10^{-3} of that in the sporadic environment. Select a spacecraft system that has a probability of 0.90 of no failures by meteoroid impact when exposed in the sporadic environment. The probability of no failures in the case when the stream is present then becomes 0.89. Second, suppose that the period of exposure of that stream were 10 times as high as in the previous example cited. This is believed not to be very probable. Nevertheless, the probability of no failures in the case without the stream would again be 0.90, and in the case when the stream is present, the probability of no failures would be 0.81. These results show that for almost all practical considerations, a relatively small change in the probability criterion results with the stream present. Therefore, it may be surmised that impact damage by sporadic meteoric matter is more significant than that

contributed by meteoric streams in the interplanetary region.

Most sporadic meteor orbits are similar to each other; that is, they are direct, and have low inclinations and large eccentricities (Ref. 18). The majority of sporadic meteors are inclined within 20 deg of the plane of the ecliptic. More than 90% of all meteoric particles are inclined within 40 deg of the ecliptic plane (Ref. 30). Many so-called sporadic meteors, having relatively very broad distributions, may belong to various not-yet-known showers (Ref. 29). The system of particles can be shown to be continuously replenished (probably by cometary contributions) according to a definite distribution function, and continuously exhausted by the operation of the Poyntning-Robertson effect alone (Ref. 32). The space density² of the particles in and near the plane of the ecliptic is also shown to be distributed as a function of solar distance.

Dust particles (micrometeoroids) tend to gravitate toward the ecliptic plane due to the planet mass concentrations in the ecliptic plane. The dispersion distance from the plane is proportional to the solar distance. Micrometeoroids tend to readily spiral into the Sun due to angular momentum energy loss caused by solar-radiation pressure. This phenomenon produces nearly circular particle orbits and also reduces the orbital eccentricity. It is expected that the concentration of particles is distributed inversely to the solar distance raised to an exponent ranging from 1 to 2, but most probably 1.5 (Ref. 12, 19). However, the value of the exponent is shown to decrease with decreasing solar distances for dust particles along the ecliptic plane and under the operation of the Poyntning-Robertson effect. This exponent is also found to have a value of less than 1.0 for particles inside the orbit of Venus (Ref. 32). Therefore, exponent values assumed greater than 1.0 will yield larger flux estimates for particles inside the 1-AU interplanetary region.

The concentration of dust at a solar distance of 1 AU in the plane of the ecliptic, and away from the Earth's dust cloud, is estimated from solar corona measurements to be 10^{-3} to 10^{-5} of that found near the Earth (Ref. 12). At this same interplanetary space location, a reasonable appraisal of the cumulative mass distribution indicates that the flux-intensity difference between the near-Earth location and the interplanetary space location increases

for decreasing particle mass (Ref. 16). Even though the dust concentration in the vicinity of the Earth's orbit may be 10^{-5} of that near the Earth, the concentration for large-sized particles—those with masses greater than about 300 g—may not be appreciably different in these two locations because of their relatively infrequent occurrence. Data from the *Mariner 2* spacecraft, which completed the Venus flyby mission, indicated that the meteoric particle concentration was not greater than 10^{-3} of that found near the Earth. For the particle size range of general interest to interplanetary missions, the particle concentration near the Earth's orbit and in the plane of the ecliptic may be 10^{-3} of that found in the near vicinity of the Earth.

The velocity of dust particles orbiting the Sun is suggested to decrease due to the Poyntning-Robertson effect (emission of the absorbed solar energy by the particle). By the same effect, it may also be predicted that the radial velocity of the dust particles into the Sun is inversely proportional to the solar distance (Ref. 12). For larger particles ($> 5\mu$), on which this perturbation has less effect, the mean meteoric particle velocity, similar to the planet velocities, is most likely to vary inversely as the square root of the solar distance.

The average particle density would most probably be similar to that of the particles accreted by the Earth. However, it is most likely that the particle density will decrease at near-solar distances due to disintegration and vaporization actions caused by solar energies. Nevertheless, an assumed constant density will be a conservative approach for this model.

It is most likely that the flux gradient of the cumulative mass distribution in regions of interplanetary space will be less than that in the near vicinity of the Earth. The mean value of the flux gradient β in Eq. (3) for the interplanetary space region will probably lie between 1.0 and 0.7. The significance of increasing the value of β is to increase the meteoroid flux for any cumulative particle mass; consequently, a greater probability of meteoroid impacts results. Therefore, if a greater flux gradient is assumed, the flux for any cumulative particle mass would be overestimated from its most probable value, thereby causing a conservative appraisal of meteoroid impact probability in the interplanetary region.

C. The Asteroid Region

Almost all asteroidal matter exists within the region of solar distances between Mars and Jupiter. Possibly there

²Cumulative particle mass in a unit volume of space for particles having a radius greater than the specified size.

are asteroids other than the known, such as Hidalgo, in the zone between Jupiter and Saturn which have escaped discovery due to their great solar distances (Ref. 1). Others, such as Eros, Hermes, and Icarus, have eccentricities which allow them to enter the region within the Earth's orbital solar distance. However, most of the asteroids which are of major concern for this model are found orbiting within the region of 2 and 4 AU solar distances; the mean distance is probably 2.8 AU. The dynamic importance of the 4 AU distance has been emphasized by other investigators (Ref. 33). Asteroids having orbits of relatively small or moderate eccentricities and inclination remain within the 2 AU region of the asteroid belt.

About 40% of the total asteroidal population move in orbits within 15 deg of inclination to the ecliptic plane and have an eccentricity ranging between zero and about 0.25. The average eccentricity of an asteroid's orbit is 0.15, and the mean inclination is 10 deg. Only a few of the orbits observed lie in the plane of the Earth's motion. Of the 1,500 major asteroidal bodies found, none move around the Sun in a retrograde direction. In this respect, the asteroidal bodies are believed to be like the planets (Ref. 1).

Investigations indicate that the number of these fragmented objects decreases with increased solar distances, suggesting that their distribution is a function of solar distance. There is also a tendency for smaller asteroids to occur farther from the Sun. For example, about 23% of the bodies existing in the region between 2.0 and 3.5 AU, and having absolute magnitudes³ between 4.0 and 8.0, occupy the zone of 3 to 3.5 AU; whereas the same 3 to 3.5 AU zone contains 95% of those asteroids with absolute magnitudes between 12.0 and 13.0 (Ref. 33).

The distribution of asteroids probably has very large gaps, due to arbitrary system positions of their pericenters, satellite longitudes, and disturbing actions of neighboring small masses (Ref. 34). Hence, the flux of asteroidal matter may be associated with streams and showers which have particles uniformly distributed along their orbit, or a cluster of particles within the orbital zone. In this respect, the asteroid zone is similar to the interplanetary regions in that it possesses many peaked flux regions which are spatially scattered. The probability of encountering a highly concentrated zone of

meteoroids in the asteroid region, however, is expected to be very small. There is presently no evidence that the particle size distributions of streams or showers extend to probable small particles. Thus, the cumulative mass distribution is not likely to be uniform or continuous. Therefore, it is difficult to establish a magnitude of flux for this region because of the considerable uncertainty as to the number of asteroids, their exact paths or orbits, the cumulative mass distribution, and their velocities.

A better understanding of the distribution of asteroids in space is obtained through studies covering cumulative meteor influxes at the Earth. It was found that large particle masses are predominantly of asteroidal origin (Ref. 35). Meteors with visual magnitudes fainter than zero are contributed primarily by cometary matter. Calculation results show that the percentage of meteors with visual magnitudes of minus 15, minus 5, and zero have a 98, 65, and 28% asteroidal origin, respectively (Ref. 36). The total meteorite contribution at the Earth by asteroidal particles may be about 1% (Ref. 37). Therefore, the debris in the asteroid region for the particle size of interest for this study largely is of cometary origin. Nevertheless, particle concentration is expected to be certainly increased due to asteroidal contributions.

Since the larger asteroidal particles are relatively much less concentrated, their contribution to the cumulative particle concentration is very small. Of primary interest is their effect on the process of secondary meteoroidal production, causing the probable existence of smaller particles. Very small-sized particles (micrometeoroids), however, are swept out of the solar system by solar-radiation pressure (Ref. 37), and therefore have probably long left the asteroid belt.

Assuming that the particle concentration of sporadic meteoric matter in space varies inversely with the solar distance, the extrapolated particle concentration in the asteroid belt would be $\frac{1}{3}$ to $\frac{1}{8}$ times the concentration of sporadic particles found in interplanetary space at a solar distance of 1 AU, but away from the Earth. However, since there may be an abundance of cometary streams existing in the asteroid region, the contribution of sporadic debris to this region by cometary particles may be as high as an order of magnitude above the extrapolated meteoric debris existing in interplanetary space. The combined constituents of cometary and asteroidal matter may increase the cumulative particle concentration in this region to 20 or 30 times that of interplanetary space, even though the number of parti-

³The brightness which the object would have when placed at a distance of 1 AU from both the Earth and the Sun.

cles of asteroidal origin may be relatively quite small for the particle size range of interest (Ref. 33, 36). However, for the model, the particle concentration shall be conservatively assumed to be 100 times that of interplanetary space concentration. It is unlikely that such an abrupt flux transition actually occurs between the asteroid region and the interplanetary region. It is more probable that this transition will be gradual; that is, from debris of lesser concentrations to fluctuations of higher concentrations occurring randomly. However, the mean integrated meteoric hazard may be statistically approached by the selection of reasonable particle concentrations for the asteroid region.

The flux gradient of the cumulative mass distribution, composed of cometary and asteroidal matter, is expected to vary with respect to cumulative particle mass. The space density is estimated to decrease inversely to the particle radius raised to the power of 4 (Ref. 38). Stone and iron fall finds on the Earth reveal that the cumulated number with mass equal to and greater than m varies inversely with m . This agrees directly with the comminution law for the process of mineral dressing (Ref. 38). The cumulative mass distribution of the meteoric matter in the asteroid belt is most likely to possess a flux gradient that is variable and not as great as that for near-Earth. It probably approaches 1.0, or less. However, it will be more conservative to assume the flux gradient to follow that for near-Earth.

Asteroidal particles generally move in direct elliptical orbits. Their mean velocities will be nearly comparable to a heliocentric circular orbital velocity at their mean solar distance. The particle flow direction, for all practical purposes, shall be considered isotropic.

The mass of the asteroids is composed of about 16.7% nickel-iron, with the remainder primarily stony-type material. The average density of asteroids may be taken as 3.5 g/cc (Ref. 38). Because of the preponderance of cometary debris in the asteroid region, the mean particle density will be much lower than 3.5 g/cc, especially for the particle size of interest for this study. A weighted mean density of the matter in this region will be assumed as 0.75 g/cc.⁴

⁴The total meteorite contribution at the Earth by asteroidal particles may be about 1%. However, if it is assumed that 10% of the total space density of the asteroid region is composed of asteroidal matter and the remaining amount composed of cometary matter which possesses a mean density of 0.443 g/cc, then the resulting mean particle density of particles in this region is 0.75 g/cc.

D. The Planetary Region

The majority of interplanetary meteoric particles deposited by cometary bodies has been estimated to be located in the zone between the Earth and Jupiter. Many cometary streams have established orbits within solar distances comparable to the asteroid belt. Thus, the Earth, Jupiter, and Mars would most likely have relatively high probabilities of accumulating meteoric debris. At great solar distances, comparable to that for Pluto, it is suspected that there would be a scarcity of interplanetary matter and asteroidal particles; zodiacal light and the appearance of bright comets would hardly be evident. Also, at such distances, meteor streams would hardly be perturbed from the nuclei of comets by meteoric scattering processes, or diverted from an established stream into sporadic meteors. For these reasons, it seems valid to postulate an extreme paucity of meteoric matter at great solar distances.

Comets originally moving nearly parallel to a planet are likely to be perturbed into orbits of direct motion with shortened periods. (Short-period comets are usually found to pass inside the orbit of Mars.) With continuing near-planetary approaches, cometary particles are perturbed and become temporary members of the planet's meteoric family. It may be hypothesized that there also exists a toroidal belt of meteoric matter, similar to that of the Earth, which contains meteoroids predominantly moving in direct motion at the planet's mean solar distance. This organization of meteoroids is very likely for Mars and especially for Jupiter. The Trojan asteroidal bodies, which have stable positions, exhibit a special case of this organization.

Sporadic meteoroids are probably more numerous near the planets than in interplanetary space because of planetary attraction. The extent of the effect of planetary gravitational forces may be shown by the irregularities and the periodic frequency of asteroidal bodies which mark orbital periods appearing to be harmonic fractions of Jupiter's orbital period. These resonant orbits may be organized through the many accumulated Jovian perturbations (Ref. 1). Cometary bodies in retrograde motion nearing a more distant planet, like Jupiter, are likely to be expelled from the solar system.

As pointed out in Section IIA, meteoric particles are perturbed and attracted from both well-defined and spurious streams only when they pass inside the tidal radius of the planet. Capture mechanics are a function of the planet's capture radius and the particle's planetocentric velocity. It is therefore reasonable to postulate

that the capturing behavior, the meteoroid distribution, and the accretion process for any planet should be analogous to that for the Earth. A quasi-equilibrium meteoric organization is assumed to be maintained by the many perturbation effects, resulting in some kind of global meteoric dust cloud peculiar to each planet (Ref. 8). For instance, apparent meteoric debris encircling Jupiter in a hypothetical equatorial belt has been proposed and is based on the argument supporting the eruption theory (Ref. 39). The precision of the experimental observations supporting this conjecture, however, is questionable (Ref. 40).

Since the capturing mechanics for meteoric particles by a planet may be analogous to that for the Earth, the distribution of particle concentration may follow a similar pattern and organization as that for near-Earth; that is, it should be a function of planetocentric distance. It will be assumed, for model simplicity, that the particle concentration varies inversely as the distance from the planet center raised to the 1.1 power. The limit to which the meteoric debris extends is the envelope of the planet's tidal radius (Ref. 42). By this reasoning, Jupiter and Saturn should have a very extensive meteoric cloud. These data are summarized in Table 2.

There is some contention that the planetary meteoric debris for both Mars and Jupiter, and especially Jupiter, is rather significant because these planets neighbor regions of apparent abundance of cometary and asteroidal matter. As discussed earlier, particles are captured primarily from low-inclined direct-orbiting matter which approach the considered planet. Since it is generally accepted that the dust particles are not likely to exist in any significant abundance in these more distant regions,

except due to secondary generation (collisional destruction), the accretion of smaller-sized meteoric matter is believed to be relatively inappreciable. For instance, the capture probability of particles less than 1 cm in radius is estimated to be rather small for Jupiter (Ref. 35, 41).

The particle concentration near the planet's surface ($c_{(\geq m)_p}$), similar to that for Earth, will be assumed to be 10^3 greater than the particle concentration found in interplanetary space at the planet's mean orbital solar distance ($c_{(\geq m)_s}$). It will also be directly proportional to the surface gravity of the considered planet relative to the Earth. This may be expressed by

$$c_{(\geq m)_p} = 10^3 \cdot c_{(\geq m)_s} \cdot \left(\frac{G_p}{G_e} \right) \quad (9)$$

The average surface gravity relative to Earth is estimated from the following equation:

$$G_p = \frac{M_p}{M_e} \cdot \left(\frac{R_e}{R_p} \right)^2 G_e \quad (10)$$

where M and R represent respectively the mass and radius of the planet. Values for these quantities are listed in Table 2.

No consideration is given to the effects displayed by planetary satellites. Their existence, however, is most likely to increase the extent of the tidal radius and the planetary debris.

The flux gradient of the accreted meteoric matter will probably differ for each planet and may be a function of the planetocentric distance. However, for the meteoroid model selected for this study, the flux gradient of

Table 2. Planetary data

Planet	Average surface gravity, G_p	Relative planet mass, M_p	Mean solar distance, 10^{-6} km	Sun-planet equigravitational distance, R_t , 10^{-3} km	Planet radius R_p , km	Dust cloud extent		Planet heliocentric velocity, km/sec	Escape velocity at near-planet, km/sec	Assumed near-planet particle, velocity, km/sec
						R_t/R_p , radii	Selected for model, radii			
Mercury	0.38	0.0543	57.9	23.3	2421	9.7	10	47.85	4.3	30.0
Venus	0.87	0.8136	108.1	193	6161	31.6	32	35.01	10.4	25.0
Earth	1.00	1.000	149.5	259	6371	40.7	65	29.76	11.2	22.0
Mars	0.39	0.1069	227.8	129	3332	38.6	40	24.11	5.1	16.0
Jupiter	2.64	318.3	777.8	24100	69892	346	400	13.05	61.0	61.0
Saturn	1.16	95.3	1426.1	24100	57532	420	450	9.64	36.7	36.7
Uranus	1.05	14.54	2869.1	19000	23701	803	800	6.78	22.4	22.4
Neptune	1.50	17.26	4495.6	32300	21535	1500	1500	5.47	25.6	25.6
Pluto	0.17	0.033	5898.9	1.85	2867	6.5	6.5	4.84	5.3	5.3

the cumulative mass distribution for each planet shall be assumed equal to that for near-Earth.

Particles orbiting the planet are assumed for this model to be predominantly in elliptical orbits, which suggests a nearly isotropic particle flow direction. This does not necessarily limit a planet from peculiarly organizing accreted matter into some form such as an equatorial belt.

The mean particle velocity near the planet will most probably be equal to the escape velocity of the particles at a low altitude from the planet's surface and will be assumed to vary inversely to the square root of the planetocentric distance. However, if the escape velocity at a low altitude is less than the particle's heliocentric velocity at the planet's mean solar distance, the mean particle velocity near the planet will most probably lie between these two velocities, similar to that proposed for the Earth. If the escape velocity is greater than the heliocentric velocity, then the escape velocity is assumed to be the mean particle velocity near the planet.

The particle density is most likely to be comparable to that found in the immediate interplanetary space environment. At near-solar distances, particle density is most likely to decrease because of the effects of solar energy. Therefore, Mercury, for instance, may accrete particles with an average density less than that found near the Earth; whereas at Mars, Jupiter, and even possibly Pluto, the density of captured meteoric matter, primarily of cometary origin, may be slightly higher than that found near the Earth, due to asteroidal contribution and to smaller solar energy effects. However, for simplicity, the average particle density accreted by a planet will be assumed to be constant and equal to that found in the near vicinity of the Earth.

E. A Meteoroid Model

From the preceding discussion of meteoroids in space, a meteoroid model covering the four defined regions is selected as follows:

The flow direction of meteoroids is isotropic throughout all space. The intercepted flux is determined by Eq. (2). The impact velocity is assumed to be equal to the mean encounter velocity of the meteoroid particles with the spacecraft. The mean particle density throughout all space is 0.443 g/cc, except in the asteroid region. The flux gradient of the cumulative mass distribution remains constant throughout space.

1. The Near-Earth Region

- a. The geocentric radius at which the meteoric environment commences is 4000 statute miles (6436 km).
- b. The particle concentration varies inversely with the geocentric distance raised to the 1.1 power.
- c. The mean particle velocity, at a geocentric distance of 4000 statute miles, is 22 km/sec and varies inversely with the square root of geocentric distance.
- d. The intercepted flux, determined by Eq. (2), is corrected for the Earth's shielding effect.
- e. The reference flux at a geocentric distance of 4000 statute miles is defined by Eq. (6).
- f. The extent of the Earth's meteoric cloud is 65 Earth radii.

2. The Interplanetary Region

- a. The particle concentration at 1 AU solar distance and away from the Earth is 10^{-3} of that found in a near-Earth region (excluding the Earth's shielding effect), and is distributed inversely with the solar distance raised to the $\frac{3}{2}$ power.
- b. The particle velocity is uniform and conforms to that of direct circular orbits in heliocentric equilibrium.
- c. The mean impact velocity of the particle with the spacecraft is the vector difference between the spacecraft and the meteoroid velocities referred to the spacecraft.
- d. The flux distribution does not vary with respect to ecliptic latitude, since the spacecraft trajectory is in the most intense flux region; that is, in the plane of the ecliptic (Ref. 43).

3. The Asteroid Region

- a. The integrated particle concentration is 100 times that of interplanetary space and extends from 2 to 4 AU solar distances.
- b. The flux is calculated similar to that for the interplanetary region.
- c. The particle velocity is uniform and conforms to that of direct circular orbits in heliocentric equilibrium.
- d. The mean particle density is 0.75 g/cc.

4. The Planetary Region

- a. The particle concentration near the planet's surface is 10^3 times that found in interplanetary space and is corrected for the planet's gravitational force.
- b. The particle concentration varies inversely with the planetocentric distance raised to the 1.1 power.
- c. The extent of the planet's meteoric cloud is to about the planet's tidal radius, as shown in Table 2.
- d. The mean particle velocity near the surface of each planet is listed in Table 2. The mean particle velocity varies inversely to the square root of the planetocentric distance and is the encountering impact velocity with the spacecraft during a planet orbital sequence.
- e. The flux calculated by Eq. (2) is corrected for the planet's shielding effect.

III. METEOROID-PENETRATION RESISTANCE ANALYSIS

Meteoroid impact damage is studied by ballistic experiments which simulate the mechanics of hypervelocity impact and aid in determining material parameters influencing such meteoroidal actions as penetration and spalling. Present-day ballistic-test equipment produces experimental projectile velocities much lower than that of most meteoroids. Extrapolation of these experimental results to the range of high meteoroid velocities is not considered reliable. Therefore, the mechanics of projectile-penetration phenomena at hypervelocities, characteristic of meteoroids, are presently best studied theoretically through the media of hydrodynamic behavior.

The sheet thickness Δ of a material, defined as that thickness required to just resist penetration of a projectile of diameter d and mass m moving with an incident velocity v normal to the surface, is proportional to the penetration depth P_c formed in a semi-infinite target by the impact of the same projectile (Ref. 44). The general form proposed for Δ as a function of v is

$$\Delta = K_1 P_c = K_1 \gamma K_2^\vartheta f(v) d \quad (11)$$

where γ is an empirical parameter which includes material and impact characteristics. The factor K_1 is defined as Δ/P_c . The value generally accepted for K_1 is 1.5. The factor K_2 is the ratio of the projectile density to the target density ρ_p/ρ_t . The function $f(v)$ may express either the projectile momentum or kinetic energy.

At high impact velocities, the penetration depth appeared to be governed by the impact forces involved; the strength of the target material was found to be of negligible order (Ref. 45). The penetration depth has been suggested to be a function of the momentum transfer, simply expressed by

$$P_c = K_3 (mv)^{1/3} \quad (12)$$

The factor K_3 is a parameter which includes material characteristics related a hydrodynamic process.

At low impact velocities, experimental penetration depth results are better correlated when the velocity function is expressed in a kinetic energy transfer form, as follows:

$$P_c = \gamma K_2^\vartheta \left(\frac{v}{M} \right)^\vartheta d \quad (13)$$

where the exponent ϑ is empirically selected as $\frac{1}{2}$. The material property term M has been suggested to be either the sonic velocity C of the undisturbed target material (Ref. 44) or a hardness property \bar{H} of the target material (Ref. 46).

However, each of the above expressions gives gross errors if extrapolated from their applicable velocity

regions. Recently, over 1700 experimental data points on cratering were statistically analyzed, resulting in an equation which appears to best express the penetration depth over the entire impact velocity range (Ref. 46). This equation shall be adopted as the penetration depth criterion used in this study and is expressed as

$$P_c = K_4 K_5^{\frac{1}{2}} d \log_e \left(1 + \frac{K_2^{2/3} v^2}{K_5 \bar{H}^2} \right) \quad (14)$$

where the constants K_4 and K_5 are suggested to be 0.6 and 4.0, respectively, for most materials (Ref. 46).

Assuming the projectile to be a spheroid, the diameter d may be expressed in terms of projectile mass m as

$$d = \left(\frac{6}{\pi} \right)^{1/3} m^{1/3} \rho_p^{-1/3} \quad (15)$$

Substituting both Eq. (15) and the relationship $\Delta = K_1 P_c$ into Eq. (14) results in

$$\Delta = K_6 \rho_p^{-1/3} m^{1/3} \log_e \left(1 + \frac{\rho_p^{2/3} v^2}{K_7} \right) \quad (16)$$

where

$$K_6 = \left(\frac{6}{\pi} \right)^{1/3} K_1 K_4 \rho_p^{-1/3} \quad (17)$$

and

$$K_7 = K_5 g_c H \rho_p^{-1/3} \quad (18)$$

Crater experiments performed at low projectile velocities indicate that circular craters are formed in target surfaces at relatively large oblique impact angles (Ref. 4). It is speculated that circular craters will predominate at higher velocities and will continue at increased oblique angles of impact. However, it is believed that the depth of penetration may be a function of the angle λ from the normal. Therefore, until further verification is available, the velocity parameter v in Eq. (16) will be replaced by the assumed cosine function of this angle, as follows:

$$v = \bar{v}(\cos \lambda)^{\eta(\lambda)} \quad (19)$$

where η is an empirical value which may be a function of λ .

A. The Variable-Flux Environment

Consider a spacecraft component exposed in the meteoroidal environment discussed in Section II. The instantaneous flux is defined by Eq. (3). An inspection of Eq. (2) and (3) reveals that at any location r the concentration and flux intensity, as well as the flux gradient may continuously change with respect to time and direction, meaning that α and β are variables with respect to time and direction. Since the mean time between probable meteoroid impacts for particles equal to and greater than a specified mass will vary, the probability of no impacts by the same particles, therefore, will also vary with respect to time. The particle velocity and density are variables with respect to time and direction. These parameters also vary with location r . However, when the mission trajectory and spacecraft performance are specified, the location r can be transformed to time t , thus making the variables functions of t and λ only.

In general, the probability of n failures during a period of time T for a system having a failure rate \dot{f} may be expressed approximately by a Poisson distribution, as follows:

$$P_{(n)} = \frac{(\dot{f}T)^n e^{-\dot{f}T}}{n!} \quad (20)$$

If the probability of no failures is sought, then Eq. (20) becomes

$$P_{(0)} = e^{-\dot{f}T} \quad (21)$$

The failure rate for a system in a meteoroidal environment is proportional to the penetrating flux projected on the vulnerable area, namely: $\dot{f} = \Phi A \cos \lambda$. The probability of no impacts then, between any time t and $t + \Delta t$, on a surface of a nonoccluded area ΔA by a meteoroid particle of mass equal to or greater than m in the direction between λ and $\lambda + \Delta \lambda$, may be expressed from Eq. (21), as follows:

$$P_{(0)}(t, t + \Delta t; \Delta A; \lambda, \lambda + \Delta \lambda) = \exp \left[-\Phi(t, \lambda) \cos \lambda \Delta A \Delta \lambda \Delta t \right] \quad (22)$$

If a meteoroid particle of mass m is of a size large enough to just cause a catastrophic failure to the component upon impact, then the probability of no catastrophic impacts on ΔA from time 0 to time T can be approximated from Eq. (22) by

$$\prod_{i=1}^n \exp \left[-\Phi(t_i, \lambda) \cos \lambda \Delta A \Delta \lambda \Delta t_i \right] \quad (23)$$

where t_i is a partition of $[0, T]$.

Thus,

$$\begin{aligned} P_{(0)}(0, T; \Delta A; \Delta \lambda) &= \lim_{n \rightarrow \infty} \exp \left[- \sum_{i=1}^n \Phi(t_i, \lambda) \cos \lambda \Delta A \Delta \lambda \Delta t_i \right] \\ &= \exp \left[- \left(\int_{t=0}^T \Phi(t, \lambda) dt \right) \cos \lambda \Delta A \Delta \lambda \right] \end{aligned} \quad (24)$$

By a similar argument, the probability of no catastrophic impacts over the entire solid angle ω is approximated by

$$\exp \left[- \sum_{i=1}^n \left(\int_{t=0}^T \Phi(t, \lambda_i) dt \right) \cos \lambda_i \Delta A \Delta \lambda_i \right] \quad (25)$$

As $\lim n \rightarrow \infty$, Eq. (25) becomes

$$P_{(0)}(0, T; \omega; \Delta A) = \exp \left[- \left(\int_{\omega} \int_{t=0}^T \Phi(t, \lambda) \cos \lambda dt d\lambda \right) \Delta A \right] \quad (26)$$

Similarly, integrating over the entire component area results in the following expression for the probability of no catastrophic impacts:

$$P_{(0)}(0, T; \omega; A) = \exp \left[- \int_{t=0}^T \iint_A \int_{\omega} \Phi(t, \lambda) \cos \lambda d\lambda dA dt \right] \quad (27)$$

The flux in Eq. (3) may be expressed in terms of Δ , rather than the particle's mass m , from the adopted relationship shown in Eq. (16). By substituting this resulting expression for Φ into Eq. (27), the armor thickness Δ may be directly related to the integrated probability of no penetrable impacts of mass m or greater in terms of all the variable meteoroidal parameters, as follows:

$$P_{(0)} = \exp \left\{ - \int_{t=0}^T \iint_A \int_{\omega} \alpha(t, \lambda) \cdot \cos \lambda \cdot \left[\frac{K_6 \rho_p(t, \lambda)^{\Phi-1/3}}{\Delta} \cdot \log_e \left(1 + \frac{\rho_p(t, \lambda)^{2/3} \bar{v}(t, \lambda)^2 (\cos \lambda)^{2\eta(\lambda)}}{K_7} \right) \right]^{3\beta(t, \lambda, m)} d\lambda dA dt \right\} \quad (28)$$

B. The Variable-Flux-Intensity Environment

The meteoroid model defined in Section IIE stipulates that the flux gradient β remains constant throughout all space and therefore is not a function of time t , direction λ , or particle mass m . In any cumulative mass distribution having a constant-flux-gradient characteristic, the existence probability P_{m_x} of all particles equal to or greater than mass m_x will not be a function of time or space, and will remain the same for any flux intensity. This existence probability may be considered as proportional to the impact probability by particles with a mass equal to or greater than m_x incident on a vulnerable area A . Consequently the flux $\Phi(t, \lambda)$ may be expressed as proportional to a reference flux $\Phi(t_0, \lambda)$. Likewise, the flux-intensity term $\alpha(t, \lambda)$ of Eq. (28) may also be expressed as proportional to a reference flux intensity $\alpha(t_0, \lambda)$. Since the flux intensity is unshielded by definition, it must be corrected for any shielding effect.

Assume that the particle density and velocity are not functions of angle λ . Furthermore, for simplicity, assume that the shielding effect S_h is also not a function of λ . For the case of the variable-flux-intensity, constant-flux-gradient environment, the probability of no catastrophic impacts can be obtained by modifying Eq. (28) into the following expression:

$$P_{(0)} = \exp \left\{ - \frac{K_6^{3\beta}}{\Delta^{3\beta}} \int_{t=0}^T \iint_A \int_{\omega} S_h(t) \alpha(t, \lambda) \cdot \cos \lambda \cdot \rho_p(t)^{\beta(3\Phi-1)} \cdot \left[\log_e \left(1 + \frac{\rho_p(t)^{2/3} \bar{v}(t)^2 \cos \lambda^{2\eta(\lambda)}}{K_7} \right) \right]^{3\beta} d\lambda dA dt \right\} \quad (29)$$

Let a dimensionless term J be introduced which shall be called the integrated angle dependency factor. It represents the influence which the integrated flux direction, including its impact effect, has on the armor thickness. Its definition is

$$J(t) = \frac{\int_{\omega} \alpha(t, \lambda) \cdot \cos \lambda \left[\log_e \left(1 + \frac{\rho_p(t)^{2/3} \bar{v}(t)^2 \cos \lambda^{2\eta(\lambda)}}{K_7} \right) \right]^{3\beta} d\lambda}{\alpha(t) \cdot \left[\log_e \left(1 + \frac{\rho_p(t)^{2/3} \bar{v}(t)^2}{K_7} \right) \right]^{3\beta}} \quad (30)$$

Incorporating the factor J into Eq. (29) results in

$$P_{(0)} = \exp \left\{ - \frac{K_6^{3\beta}}{\Delta^{3\beta}} \int_{t=0}^T \iint_A J(t) S(t) \alpha(t) \rho_p(t)^{\beta(3\Phi-1)} \cdot \left[\log_e \left(1 + \frac{\rho_p(t)^{2/3} \bar{v}(t)^2}{K_7} \right) \right]^{3\beta} dA dt \right\} \quad (31)$$

C. The Constant-Flux Environment

In an environment of uniformly distributed meteoroid particles, a certain mean time between interception of meteoroid particles with mass equal to or greater than a given mass will result. The parameters in Eq. (3) for this uniform flux distribution do not change with respect to time. Therefore, there will be a certain probability of meteoroid impact associated with a spacecraft component according to Eq. (31), where all the meteoroidal parameters are no longer functions of time but take on mean constant values. Let the values of the parameters at time t be the same as that at a reference time t_0 . The flux intensity $I(t)$ becomes by definition unity. From Eq. (31), the probability of no catastrophic impacts by a mass m or greater for the case where the variables each remain at constant values over a period of time T is found to be

$$P_{(0)} = \exp \left\{ - \left(\frac{\alpha K_6^{3\beta} J S_h \rho_p^{\beta(3\Phi-1)} A T}{\Delta^{3\beta}} \right) \left[\log_e \left(1 + \frac{\rho_p^{2/3} \bar{v}^2}{K_7} \right) \right]^{3\beta} \right\} \quad (32)$$

Equation (32) may be rewritten as

$$\Delta = K_6 \rho_p^{\Phi-1/3} \left(\frac{J S_h \alpha A T}{-\log_e P_{(0)}} \right)^{1/(3\beta)} \log_e \left(1 + \frac{\rho_p^{2/3} \bar{v}^2}{K_7} \right) \quad (33)$$

D. Application of Section IIIB

Let two missions, subscripted c and v , having constant- and variable-flux-intensity environments, respectively, be compared to each other in terms of equal mission times and equal probabilities of no catastrophic impact for a component of vulnerable area A , meaning that $P_{(0)v} = P_{(0)c}$. For convenience, let the mission containing a constant-flux-intensity environment be a near-Earth orbital mission. Furthermore, let it dictate the reference values at time t_0 . Let the mission possessing a variable-flux-intensity environment be a specified interplanetary mission.

The expression for the probability of no impacts by a mass m or greater for an area exposed in this environment is given by Eq. (32) in terms of the armor thickness Δ . A similar expression is given by Eq. (31) for a variable-flux-intensity, constant-flux-gradient environment. By equating Eq. (31) and (32), equal probability of no catastrophic impact criteria for each case is satisfied, and is given by

$$\begin{aligned} -\log_e P_{(0)} &= \frac{A T J(t_0) S_h(t_0) \alpha(t_0)}{\Delta_c^{3\beta}} \cdot K_6^{3\beta} \rho_p(t_0)^{\beta(3\Phi-1)} \cdot \left[\log_e \left(1 + \frac{\rho_p(t_0)^{2/3} \bar{v}(t_0)^2}{K_7} \right) \right]^{3\beta} \\ &= \frac{A K_6^{3\beta}}{\Delta_v^{3\beta}} \int_{t=0}^T J(t) S_h(t) \alpha(t) \rho_p(t)^{\beta(3\Phi-1)} \cdot \left[\log_e \left(1 + \frac{\rho_p(t_0)^{2/3} \bar{v}(t_0)^2}{K_7} \right) \right]^{3\beta} \end{aligned} \quad (34)$$

The protection requirement ratio \mathcal{R} , defined as the ratio of armor thickness required for a specific interplanetary meteoric exposure Δ_v to that required for a near-Earth constant flux Δ_c can be evaluated by rearranging Eq. (34) as follows:

$$\mathcal{R} = \frac{\Delta_v}{\Delta_c} = \left\{ \frac{1}{T} \int_{t=0}^T \left(\frac{J(t)}{J(t_0)} \right) \left(\frac{S_h(t)}{S_h(t_0)} \right) \left(\frac{\alpha(t)}{\alpha(t_0)} \right) \left(\frac{\rho_p(t)}{\rho_p(t_0)} \right)^{\beta(3\Phi-1)} \cdot \frac{\left[\log_e \left(1 + \frac{\rho_p(t)^{2/3} \bar{v}(t)^2}{K_7} \right) \right]^{3\beta}}{\left[\log_e \left(1 + \frac{\rho_p(t_0)^{2/3} \bar{v}(t_0)^2}{K_7} \right) \right]^{3\beta}} dt \right\}^{1/(3\beta)} \quad (35)$$

The expression within the integral of Eq. (35) is interpreted as a relative damaging potential of the meteoric hazard. It is a measure of the flux intensity combined with the physical and kinetic characteristics of the noted meteoric parameters. Let this dimensionless expression be called the normalized flux intensity and denoted by the symbol $I(t)$. From Eq. (35), the quantity $I(t)$ is

$$I(t) = \left(\frac{J(t)}{J(t_0)} \right) \left(\frac{S_h(t)}{S_h(t_0)} \right) \left(\frac{\alpha(t)}{\alpha(t_0)} \right) \left(\frac{\rho_p(t)}{\rho_p(t_0)} \right)^{\beta(3\Phi-1)} \cdot \frac{\left[\log_e \left(1 + \frac{\rho_p(t)^{2/3} \bar{v}(t)^2}{K_7} \right) \right]^{3\beta}}{\left[\log_e \left(1 + \frac{\rho_p(t_0)^{2/3} \bar{v}(t_0)^2}{K_7} \right) \right]^{3\beta}} \quad (36)$$

The ratio \mathcal{R} may then be simply expressed as

$$\mathcal{R} = \left[\frac{\int_{t=0}^T I(t) dt}{T} \right]^{1/(3\beta)} \quad (37)$$

The factor J , defined by Eq. (30), has been evaluated for an isotropic flux environment and is shown by Fig. 6 as a function of impact velocity and meteoroid density. A similar J factor has been evaluated (Ref. 47) for a near-Earth orbital environment by assuming the flux to vary longitudinally and latitudinally, as shown in Fig. 1 and 2, with a selected penetration model described by Eq. (13). However, as pointed out in Section IIA, the time exposure in the very-near-Earth environment for most interplanetary trajectories is relatively small, and for computation simplicity, the longitudinal flux variations may be neglected by simply integrating the flux exposure to yield the mean flux value. Furthermore, the flux direction, for all practical purposes, will most probably be isotropic.

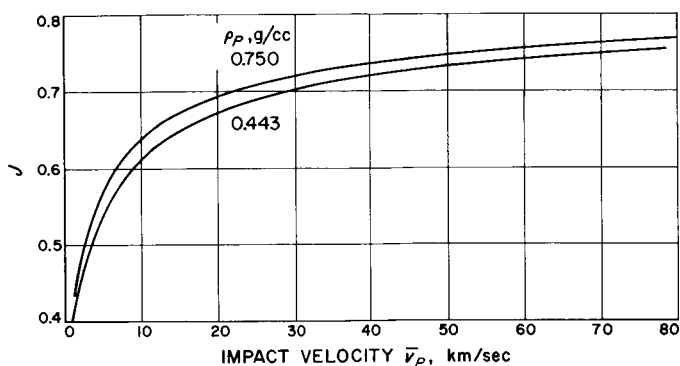


Fig. 6. Factor J vs meteoroid velocity for meteoroid-density parameters

The armor thickness required for a near-Earth orbital mission may be evaluated by Eq. (33) when proper values for the parameters are introduced. These values may be selected as follows:

1. Equation (7) adopts the α and β values at 6.62×10^{-15} and 1.34, respectively (Ref. 19). The α value is not corrected for the Earth's shielding effect.
2. The power φ is equal to $\frac{2}{3}$ (Ref. 46).
3. The factor J is selected as 0.6814 at $\bar{v} = 22$ km/sec.
4. The mean impact velocity is assumed to be 22 km/sec.
5. The average meteoroid density $\rho_p(t_0) = 0.443$ g/cc.
6. The H_t for materials most generally used for spacecraft will be assumed to be 110 kg/mm².

7. The target density generally ranges from about 1.9 to 7.7 g/cc.

When these selected values are introduced into Eq. (33), and ρ_τ takes on units of g/m³, the armor thickness Δ_e in meters may be expressed as

$$\Delta_e = (0.562) (10^{-5}) K_s \left(\frac{AT}{-\log_e P_{(0)}} \right)^{0.248} \quad (38)$$

where K_s is a factor that includes the density characteristic of the target material. Numerical values are shown in Fig. 7.

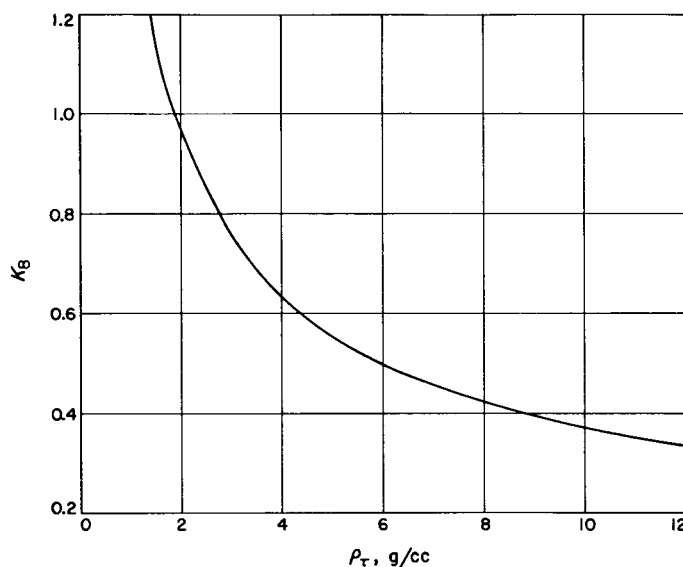


Fig. 7. Factor K_s vs target-material density

IV. A METEOROID FLUX-INTENSITY PROFILE FOR A PLANETARY MISSION

Suppose that a planetary mission to Jupiter is to be performed by a conceptual nuclear-electric spacecraft (Ref. 48). There are three phases of flight trajectory which must be considered for this spacecraft. As shown in Fig. 8, there is the spiral-out to escape, the heliocentric trajectory, which includes the asteroid region, and the planetary rendezvous and spiral-in to desired orbit. The meteoroid concentrations and spatial distribution covering the damaging size range of meteoroids in these zones have been discussed in Section II.

During the initial flight period, the spacecraft becomes vulnerable to the Earth's meteoric hazard when the aerodynamic shroud of the booster is ejected. This may occur at an altitude of about 45 km and at a time period of under 3 min after launch. The time required after launch to reach 1000 km is about 25 min. The spiral-out trajectory to escape the Earth commences at about 6 hr after launch. Since the spiral-out-to-escape phase takes over 70 days, the time period of the initial trajectory phases of booster-spacecraft is relatively so small that they may be neglected for this study. Thus the spacecraft shall be assumed to commence its spiral-out-to-escape trajectory at the altitude of the greatest meteoroid concentration (geocentric distance of 6436 km) so that a more severe meteoric flux exposure may be evaluated.

The spacecraft trajectory during the spiral-out from Earth is shown by Fig. 9. The variable-thrust optimum

trajectory calculations are based on a typical spacecraft initial acceleration of 10^{-3} m/sec² (Ref. 49). Point *a*, shown in Fig. 9, is the approximate point at which transition from the spiral-out to heliocentric transfer occurs. This trajectory is typical for almost all interplanetary and planetary missions and will be assumed as such for this study.

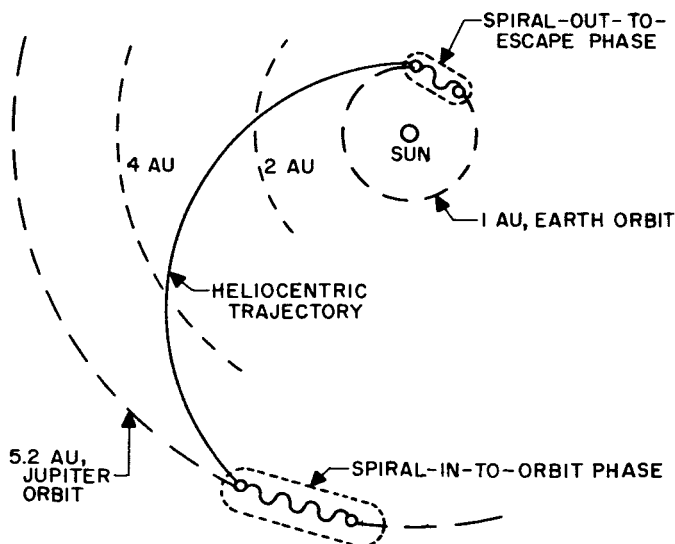


Fig. 8. Jupiter orbiter mission plan

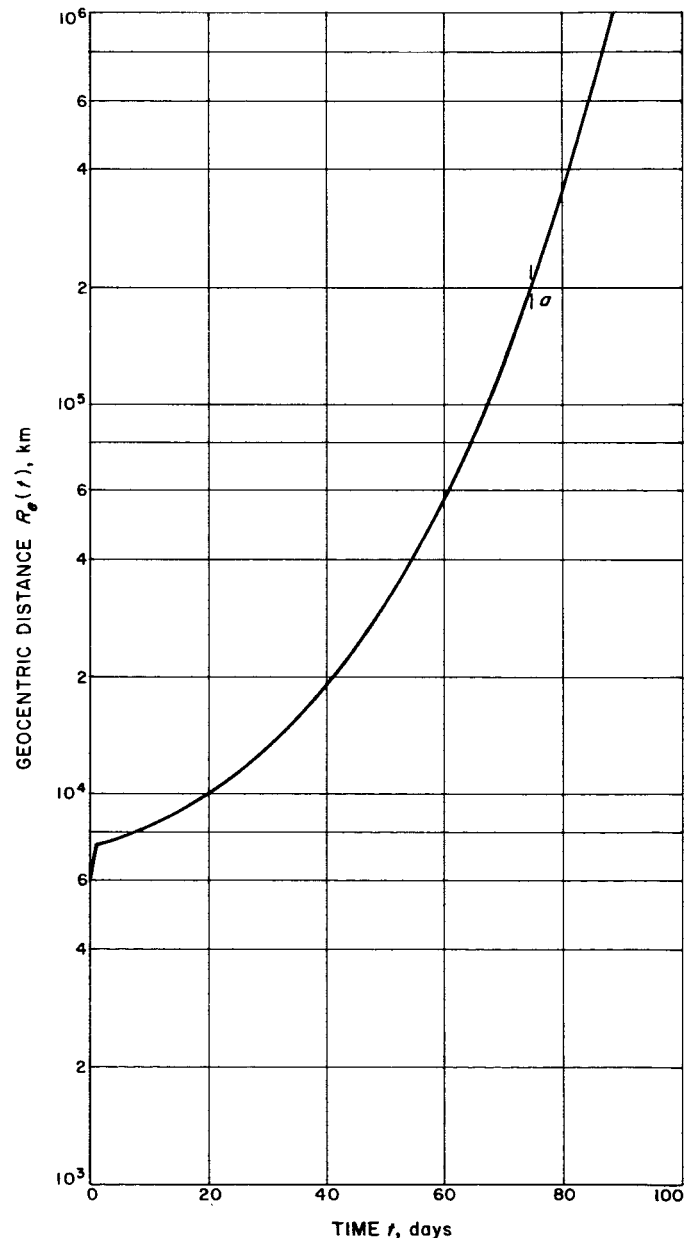


Fig. 9. Spiral-out from Earth trajectory

Table 3. Spacecraft heliocentric trajectories

Planet	Type of mission	Time ^a , days	Solar distance ^b , 10 ⁸ km
Solar	Probe	0	149.6
		32	152.5
		64	163.4
		128	193.4
		224	162.6
		256	103.3
		272	049.7
		280	014.96
Mercury	Flyby	48	145.2
		96	114.3
		128	071.9
		142	057.9
Venus	Encounter	32	146.8
		64	137.3
		128	111.6
		162	108.2
Mars	Encounter	64	162.0
		128	193.4
		160	206.5
		199	216.0
Jupiter	Encounter	64	160.9
		160	262.8
		320	501.5
		512	723.8
		645	778.3
Saturn	Encounter	96	184.4
		192	324.1
		352	632.2
		576	1064.1
		736	1302.0
		935	1427.0
Uranus	Flyby	96	184.8
		192	345.6
		384	848.9
		512	1264.3
		640	1724.9
		768	2216.7
		932	2869.6
Neptune	Flyby	288	588.0
		576	1570.7
		780	2535.0
		1024	3607.6
		1202	4496.6
Pluto	Flyby	192	351.2
		384	892.7
		576	1616.7
		768	2484.3
		992	3633.1
		1184	4696.4
		1394	5900.0

^aTime is from Earth escape (75 days).
^bInitial spacecraft acceleration is 10⁻³ m/sec².

The heliocentric trajectory can be quite accurately obtained by knowing the specified performance of the spacecraft and the respective solar and planetary gravitational forces. The heliocentric trajectory for various missions, including that for the Jupiter mission, is described in Table 3. The entire trajectory profile for a Jupiter orbiter mission is shown in Fig. 10.

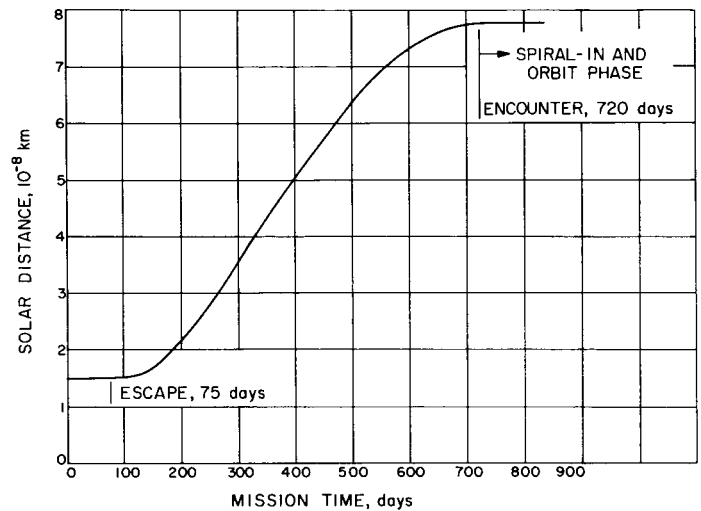


Fig. 10. Jupiter orbiter mission trajectory

When the spacecraft is captured by a planet, it will assume kinematics defined by the following equations (Ref. 50):

The planetocentric distance R_p is

$$R_p = \frac{a(1 - \epsilon^2)}{1 + \epsilon \cos \Theta} \quad (39)$$

where a is the major radius of the elliptical orbit, and Θ is the true-anomaly angle.

The spacecraft velocity $v_{s/c}$ relative to the planet is

$$v_{s/c}^2 = \mu \left(\frac{2}{R_p} - \frac{1}{a} \right) \quad (40)$$

where μ is a gravitational parameter for the planet.

The eccentricity ϵ of the orbit is

$$\epsilon = \frac{R_{p1} - R_{p2}}{R_{p1} + R_{p2}} \quad (41)$$

where R_{P1} and R_{P2} are the farthest and nearest planetocentric approaches, respectively.

The spacecraft elliptical orbit around Jupiter is selected to have a perigee of 800,000 km and an eccentricity of 0.5. From Eq. (39)–(41), the planetocentric distance-time profile may be found and incorporated to obtain the meteoroid flux-intensity profile for an orbital cycle.

The instantaneous meteoroid flux encountered by a spacecraft during an interplanetary mission may be synthesized from the mission trajectory and the meteoroid

characteristics and distribution defined by the meteoroid model. This exposure may be normalized and expressed as a flux intensity provided that the flux gradient at any given time is identical to the referenced flux gradient. The meteoroid model includes this conditional assumption.

The profile of the normalized flux intensity $I(t)$ from Earth to the vicinity of Jupiter is estimated by the incorporation of the meteoroid model, the spacecraft trajectory (Fig. 10), and Eq. (36) described in Section III. The integration of this profile, shown in Fig. 11, for the

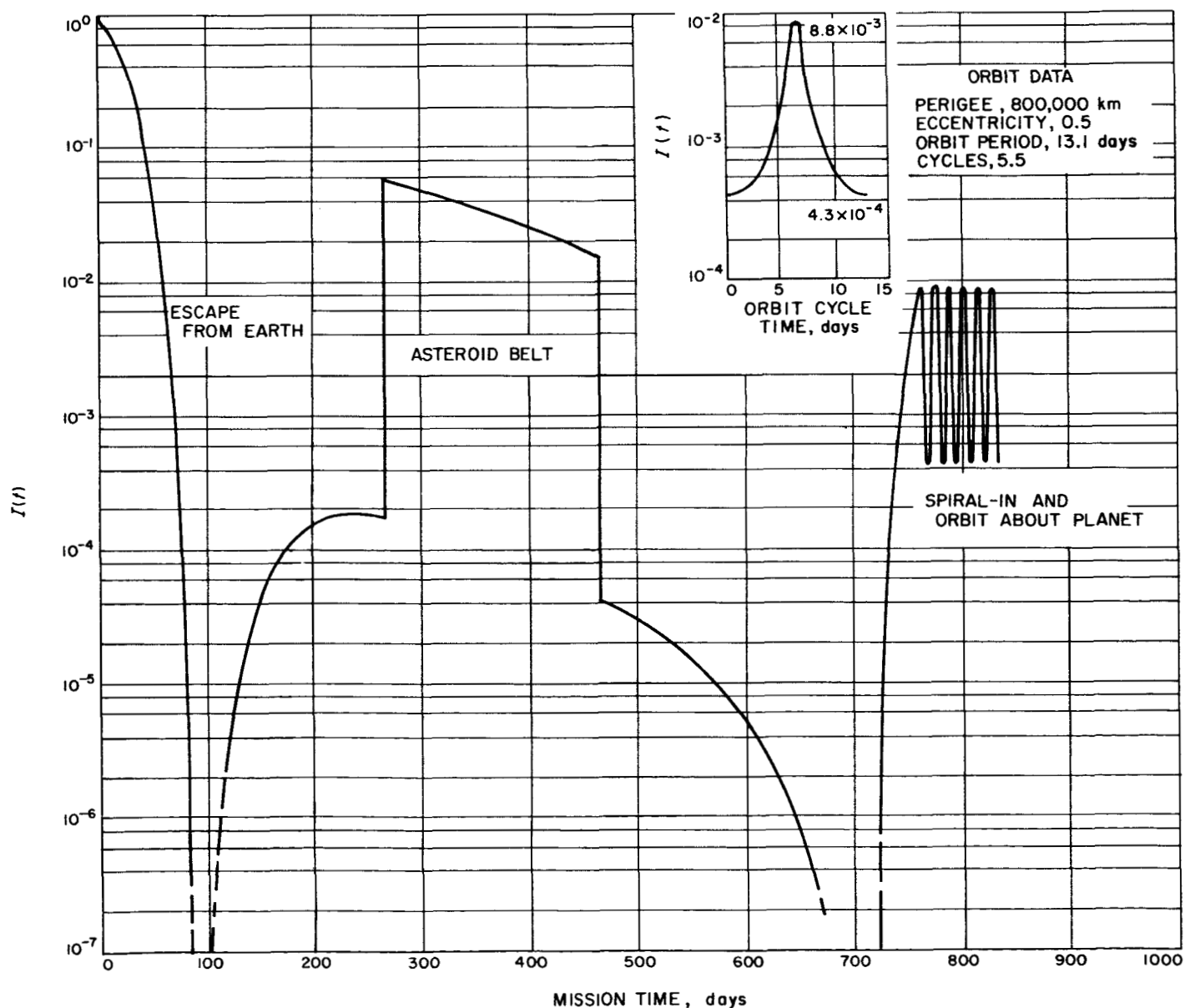


Fig. 11. Jupiter orbiter flux-intensity profile

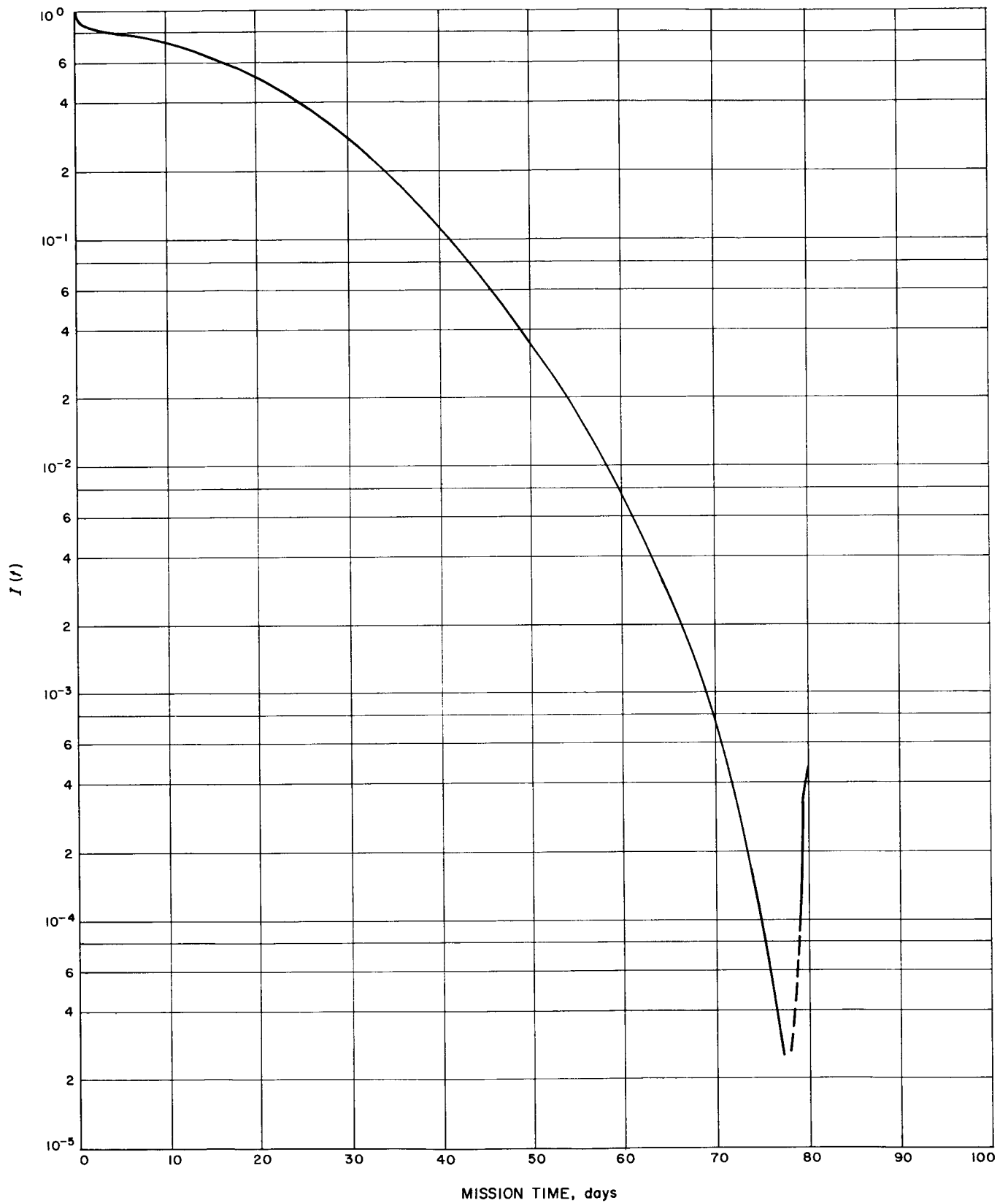


Fig. 12. Lunar encounter flux-intensity profile

Jupiter orbiter mission, results in the total meteoric damage exposure used to evaluate the protection requirement ratio \mathcal{R} .

The profile shown in Fig. 11 indicates that a very marked decline of flux intensity exists at two zones: during the transition from spiral-out from Earth to heliocentric transfer and at rendezvous with the target planet. At these two zones, the spacecraft's velocity vector is almost equal to a direct heliocentric circular equilibrium condition. Based on the meteoroid model, meteoroids are also in a direct heliocentric circular equilibrium condition. Since the probable number of meteoroids intercepted is proportional to the relative velocity of the spacecraft in its trajectory and the meteoroids, the meteoric flux is greatly reduced at these two zones, which causes the sharp decline of the intensity shown in Fig. 11. Another

reason for the sharp decrease of flux intensity is that the damaging effect of the meteoroid particle is significantly decreased at these resultant mean impact velocity levels.

Flux-intensity profiles for other interplanetary missions are shown in Fig. 12-20. In Fig. 14, the point marked X is that point at which the spacecraft would encounter Mercury. From point X, if the proper guidance is employed, a spiral-in to a highly elliptical orbit may be made, similar to that shown for Jupiter. Venus and Mars orbiter profiles, shown in Fig. 15 and 16, respectively, assume circular orbits. Their spiral-in trajectories are described in Table 4.

The technique developed in Section III uses these profiles to evaluate the system protection requirement necessary to resist meteoroid penetration damage.

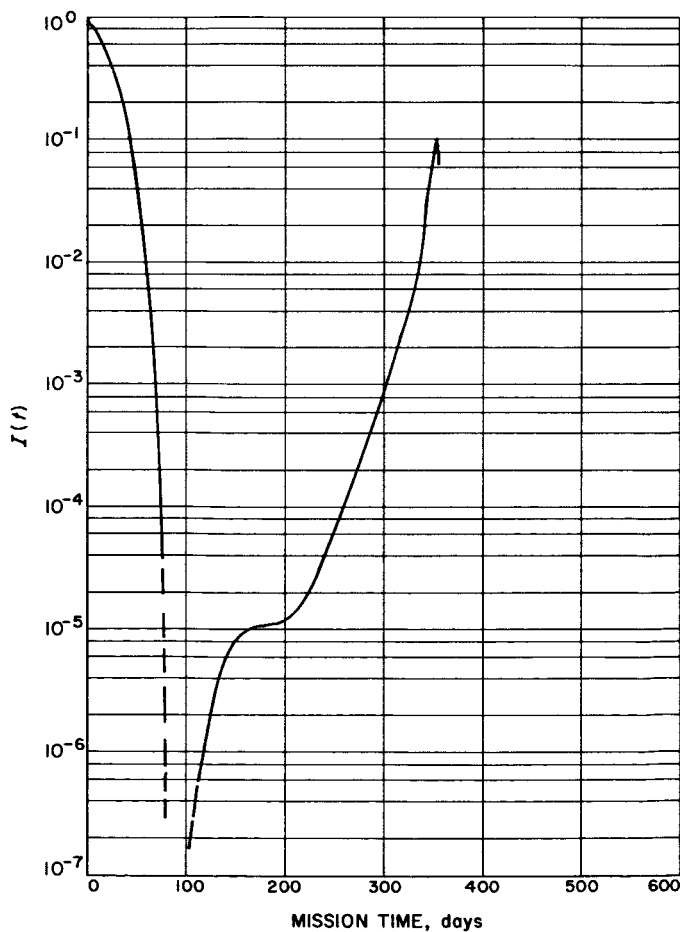


Fig. 13. Solar probe flux-intensity profile

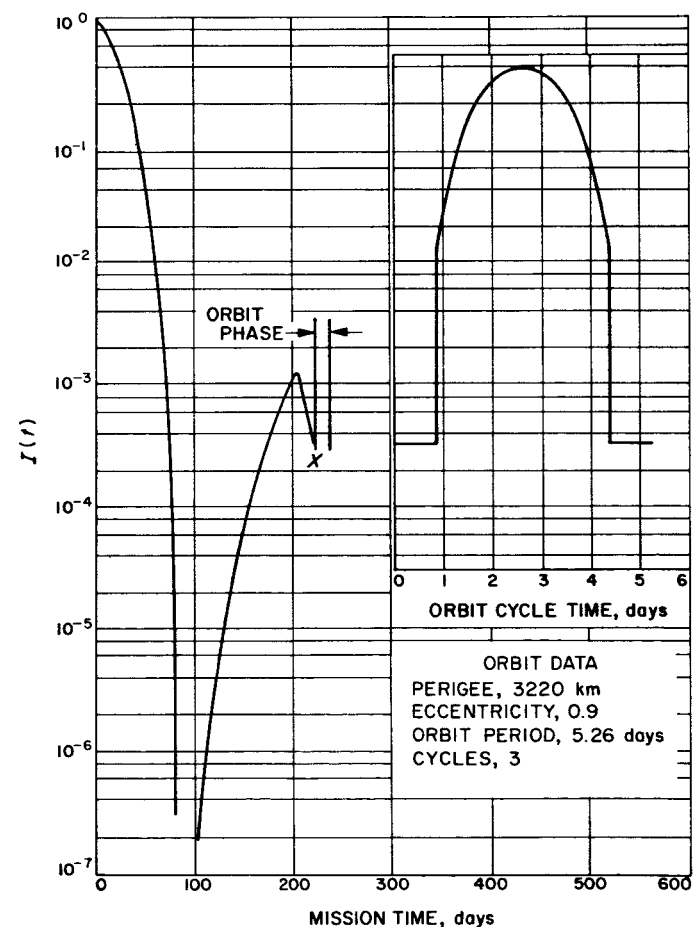


Fig. 14. Mercury orbiter and flyby flux-intensity profile

Table 4. Spacecraft planetary spiral-in trajectories

Planet	Time ^a , days	Altitude, 10 ⁻⁶ m	Planet	Time ^a , days	Altitude, 10 ⁻⁶ m
Venus	Capture	—	Mars	Capture	—
	2	887.5		4	140.2
	12	117.6		9	40.2
	22	44.2		14	17.1
	32	21.7		19	8.6
	42	12.2		24	4.5
	52	6.1		29	2.2
	62	2.9		34	0.8
	72	0.8			

^aSpacecraft deceleration is 10⁻³ m/sec².

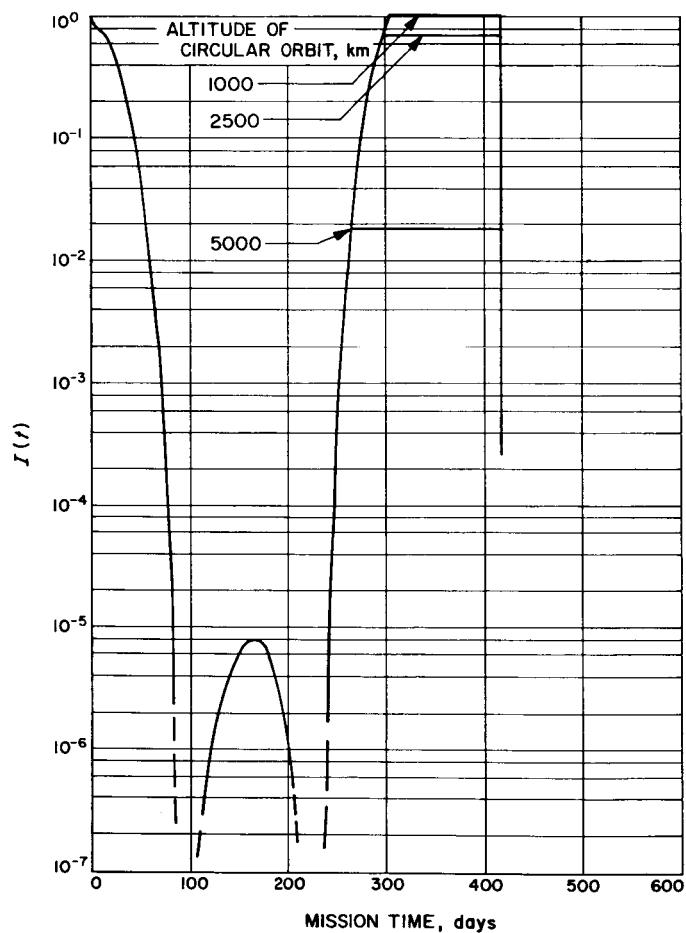


Fig. 15. Venus orbiter flux-intensity profile for various circular orbits

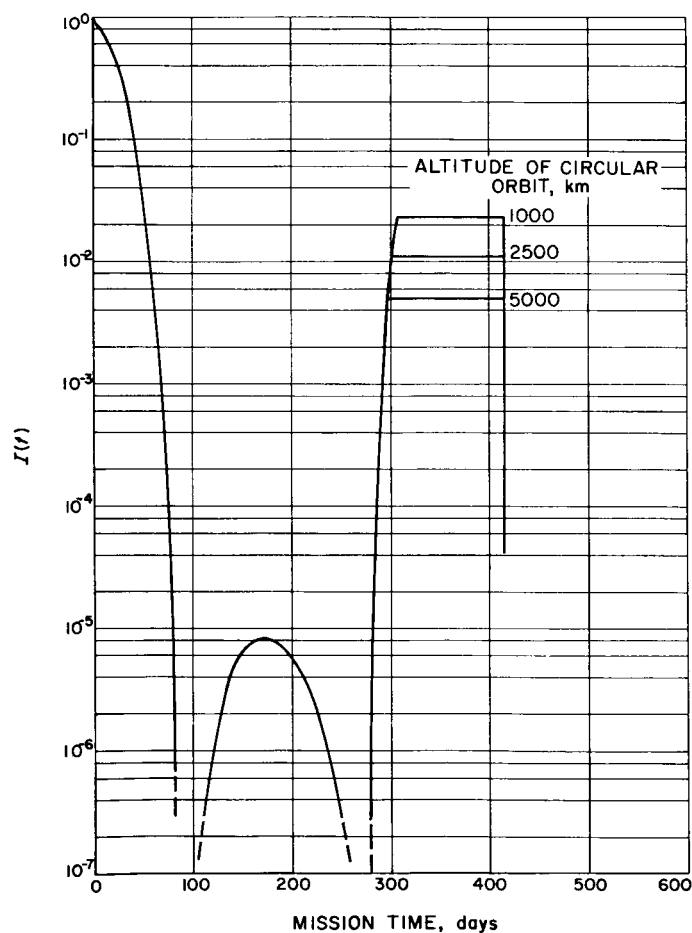


Fig. 16. Mars orbiter flux-intensity profile for various circular orbits

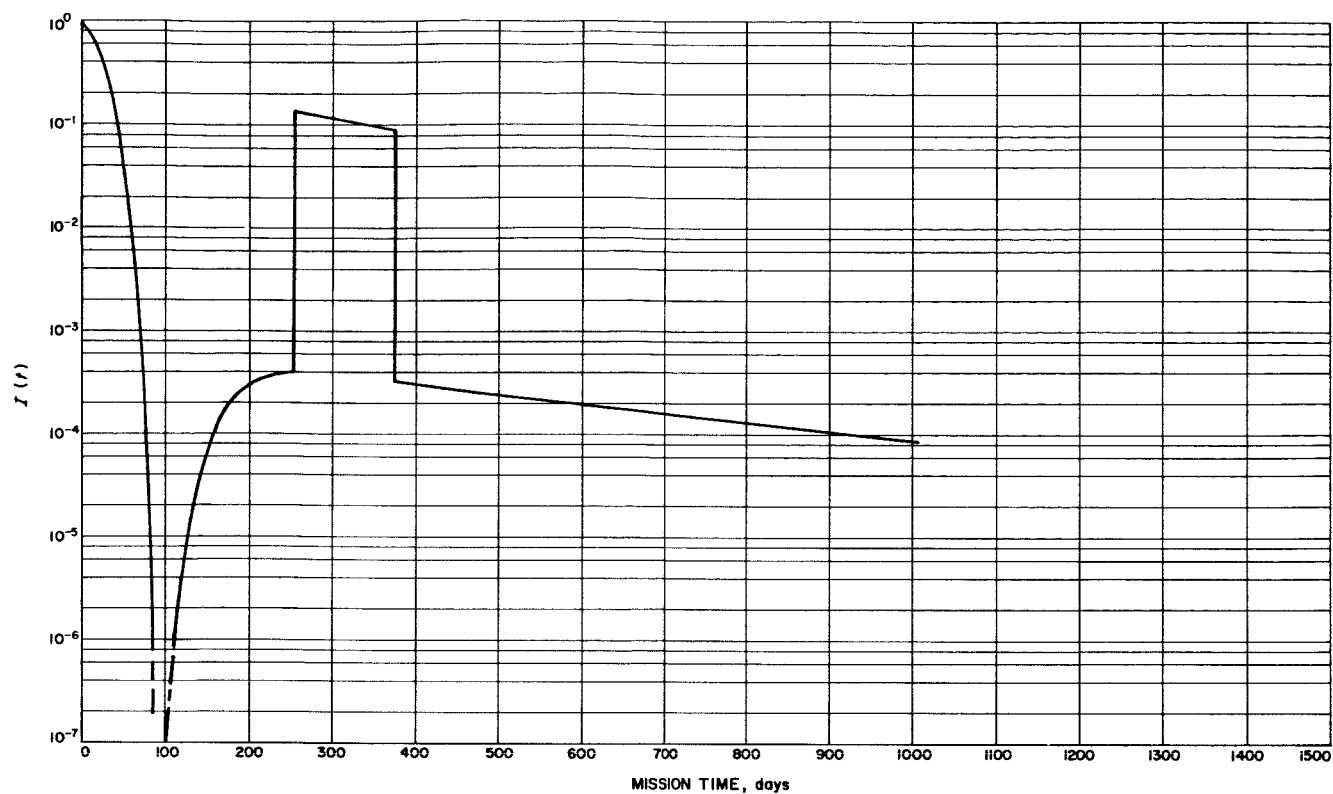


Fig. 17. Uranus probe flux-intensity profile

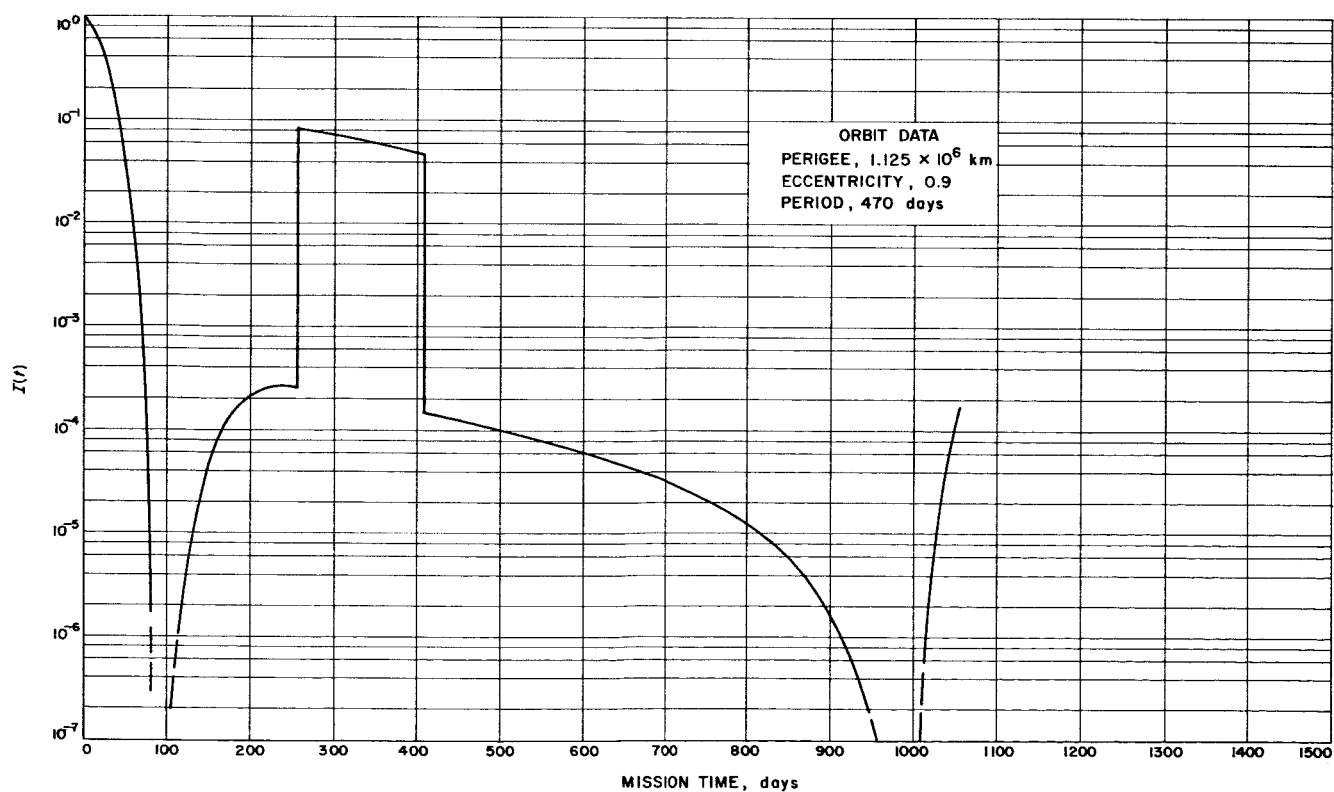


Fig. 18. Saturn orbiter flux-intensity profile

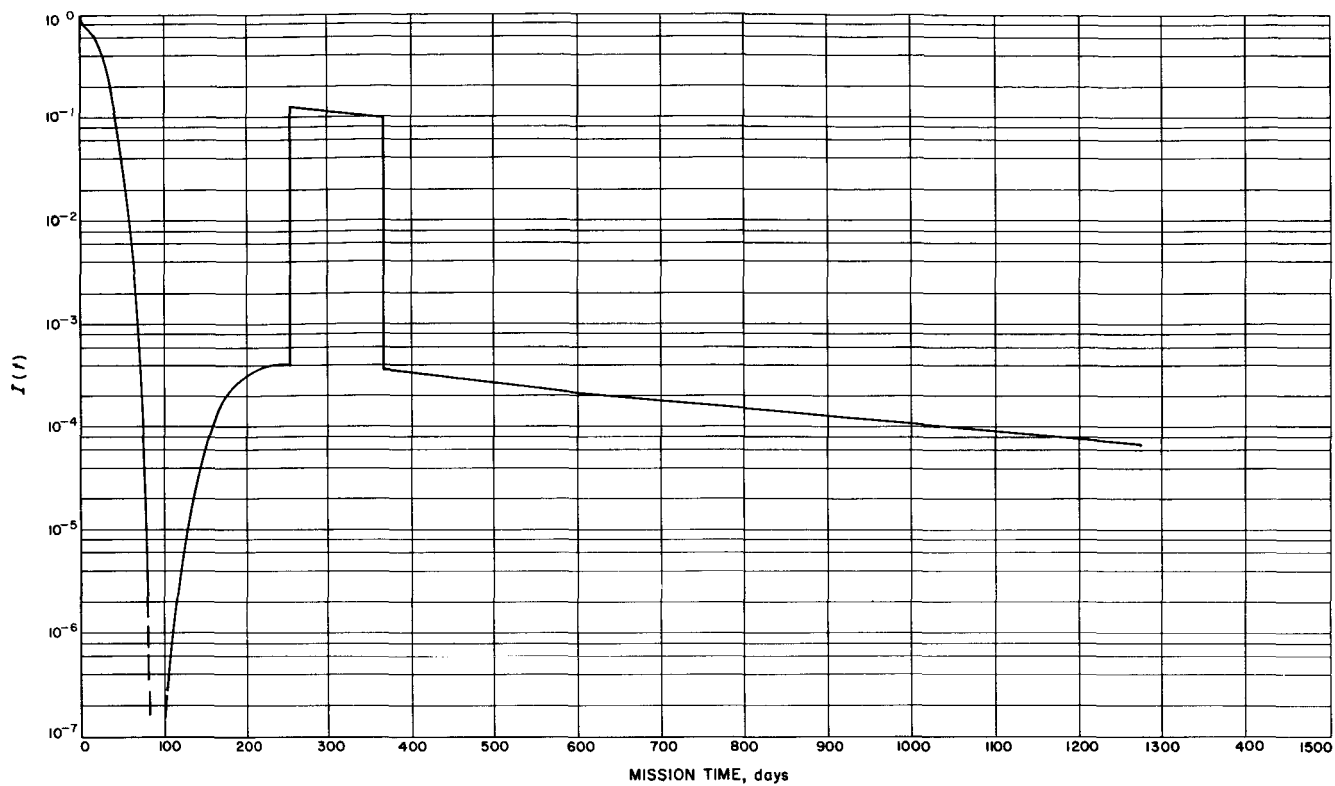


Fig. 19. Neptune probe flux-intensity profile

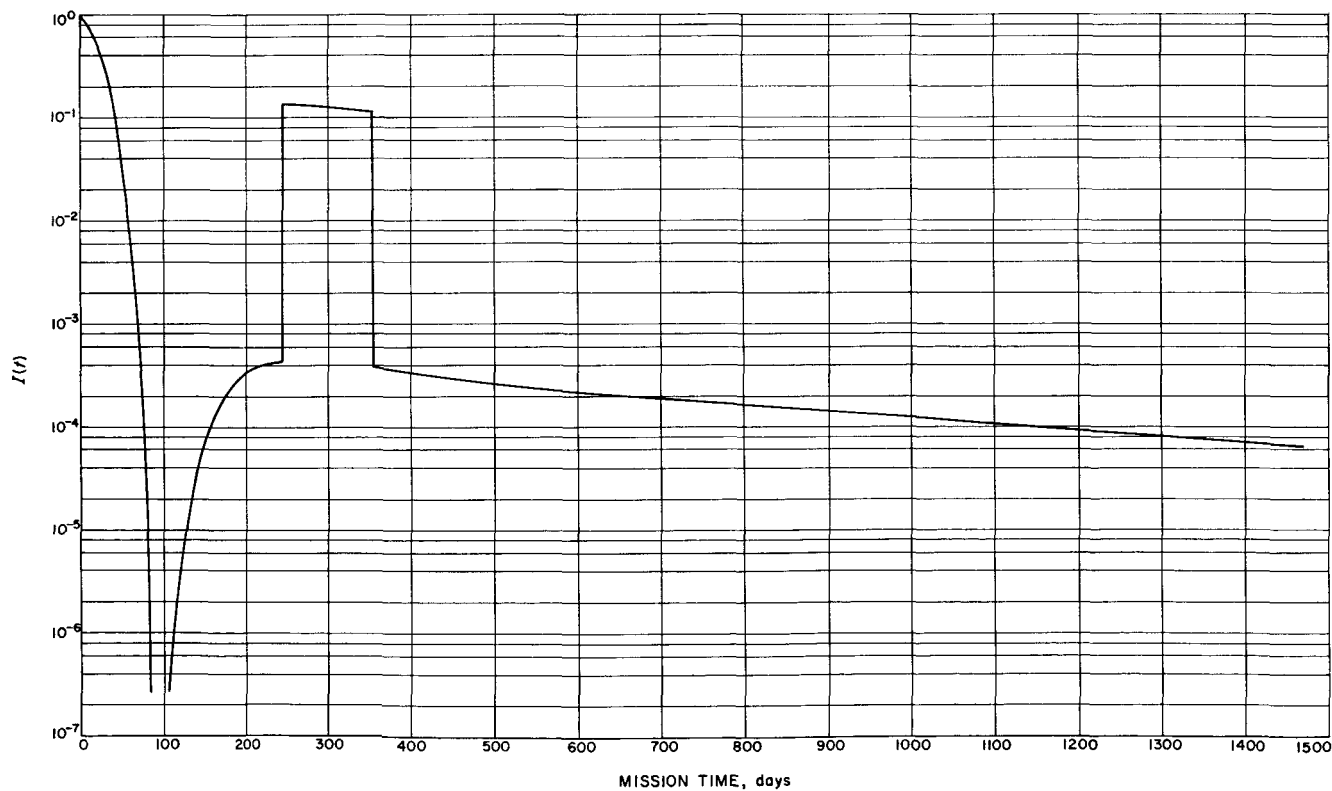


Fig. 20. Pluto probe flux-intensity profile

V. PROTECTION REQUIREMENT ESTIMATES

A. Vulnerable Area

The vulnerable area of a nonoccluded component, when exposed in a uniform and isotropic flux environment, is simply the outside surface area A_0 . However, the component's outer wall, of a finite thickness, has an integrated probability of no catastrophic impacts $P_{(0)}$ in this same meteoroid flux. Let this component have a variable wall thickness $\Delta(A)$. The $P_{(0)}$ term can be computed by integrating Eq. (31) over the entire outside surface, as follows:

$$-\log_e P_{(0)} = \frac{1}{K_9} \iint_{A_0} \frac{dA}{\Delta(A)^{3\beta}} \quad (42)$$

where K_9 is a constant which combines the physical and material parameters as defined by Eq. (31).

If the mean wall thickness of the component is $\bar{\Delta}$, and the desired overall probability of no catastrophic impacts is $\bar{P}_{(0)}$, it can be shown by Eq. (31) that the effective vulnerable area A_{eff} is

$$A_{eff} = K_9 \cdot (\bar{\Delta})^{3\beta} \cdot (-\log_e \bar{P}_{(0)}) \quad (43)$$

Then

$$A_{eff} = (\bar{\Delta})^{3\beta} \left(\frac{-\log_e \bar{P}_{(0)}}{-\log_e P_{(0)}} \right) \cdot \iint_{A_0} \frac{dA}{(\Delta(A))^{3\beta}} \quad (44)$$

A valid comparison of the relationship of A_{eff} with A_0 in Eq. (44) will be obtained if the probabilities of no catastrophic impacts by a mass of m or greater are equal; namely, $P_{(0)} = \bar{P}_{(0)}$. Eq. (44) then becomes

$$A_{eff} = \iint_{A_0} \left(\frac{\bar{\Delta}}{\Delta(A)} \right)^{3\beta} dA \quad (45)$$

The vulnerable area per tube and unit tube length for a nonoccluded tube-fin geometry may be approximated by

$$A_{eff} = \pi \cdot \overline{OD} - 2\delta \quad (46)$$

where δ is the root thickness of the fin and does not exceed $\frac{1}{8}$ of the outside tube diameter \overline{OD} . If δ does exceed this limit, then Eq. (45) should be used to obtain a better estimate of A_{eff} .

B. Heat-Rejection Radiator Mass

A heat-dissipation system is required for a nuclear-electric power-generating system. Heat rejection to the space environment by a thermal radiator is found to be the most effective method for the range of most proposed nuclear-electric systems. A typical 500-kwe nuclear-electric spacecraft (Ref. 48), shown in Fig. 21, can be designed to capably perform all the interplanetary missions designated in Table 3. The components most vulnerable to meteoric hazards are the heat-rejection radiators. There are three such radiator systems: (1) the primary (condensing) radiator for the 2-loop power-generation thermodynamic cycle; (2) the subcooler radiator required for the alternator equipment cooling; and (3), the secondary radiator employed for electronic component cooling. Of the three systems, the primary radiator is found to be the most vulnerable to meteoroid impact because of its larger area. When armored by the usual methods, which use a constant near-Earth flux, the primary radiator mass may be as much as 33% of the total mass of the power-generating system, and as much as 15% of the total spacecraft mass. Therefore, the primary radiator, because of its critical vulnerability and massiveness, requires careful design attention.

A finned tube is the most economical geometry for heat rejection at the radiator temperature level proposed for this spacecraft (Fig. 21). The optimum transfer-tube configuration can be shown to be cylindrical. The average primary radiator heat-rejection tube temperature is rated at 1200°F. Beryllium is utilized for the armor and constant-temperature gradient fin (Ref. 51). The columbium liner thickness, rated to be about 4% of the inside tube diameter to meet intube-fluid compatibility requirements, is assumed to not contribute any protection against meteoroid impact damage. The vapor supply and condensate headers are constructed of columbium to be structurally compatible with the tube liner used. Beryllium is not applied to the headers since they are rated to possess sufficient armor protection comparable to the radiator tube criterion. The biform primary radiator is divided into six sections on each side. The tube lengths in all the sections are the same so that uniform and better-controlled vapor-condensate fluid flow may be achieved.

The vulnerable area for the primary radiator was found by evaluating Eq. (46). The armor thicknesses Δ_e are obtained from Eq. (38) for various near-Earth orbital mission times and are shown in Table 5 for a $P_{(0)} = 0.95$.

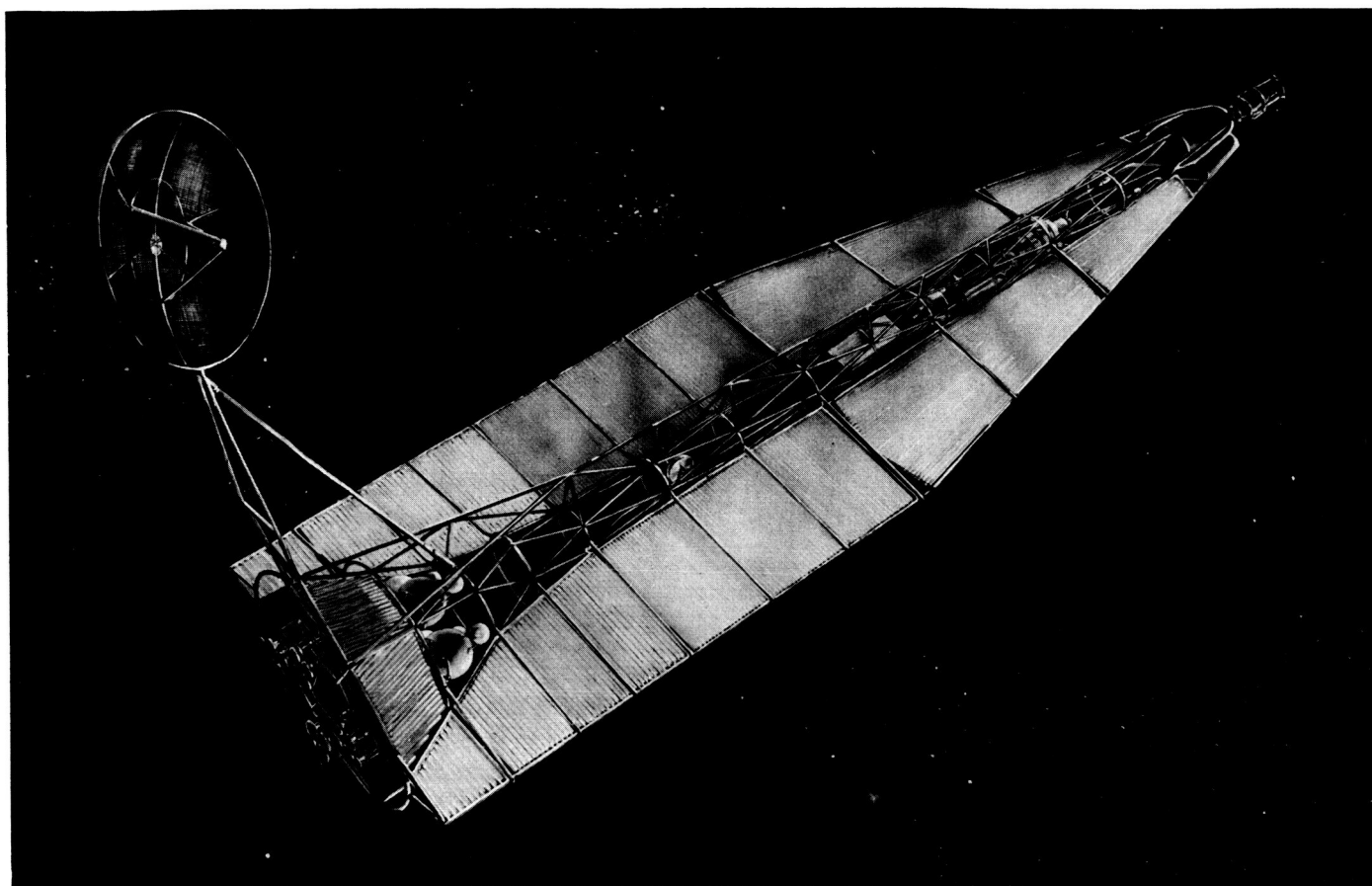


Fig. 21. 500-kwe nuclear-electric space cruiser

From the listed protection requirement ratios \mathcal{R} , the armor thicknesses Δ_v for various described missions are obtained and also shown in Table 5.

Should the radiator systems be standardized to offer mission flexibility, the radiator armor thickness will remain essentially constant regardless of the selected mission. This radiator system would offer a different probability of no catastrophic impacts for each selected mission. The standardized armor thickness should be specified such that a reasonable minimum designed probability of no catastrophic damage will result for the mission containing the greatest expected meteoroid hazard. For less hazardous missions, the probability of no catastrophic damage would increase. For instance, a standardized armor thickness of 1 mm (40 mils) would yield a $P_{(0)}$ of about 0.71 for the primary radiator system during a Venus orbital mission, and a $P_{(0)}$ of about 0.93 for a Saturn mission. The $P_{(0)}$ estimates for all the missions are shown in Table 5 for standardized armor thicknesses of beryllium varying from 1 to 3 mm.

When the operating reliability of the power-generating system includes meteoroid impact effects, particularly the probability of no catastrophic impacts of the radiator system, the overall system reliability is decreased. If the estimated $P_{(0)}$ value is low, the overall system reliability is seriously affected. An increase of the standardized armor thickness of the radiator system produces only a slight increase in system mass but a large increase of system reliability. For instance, if the armor thickness is changed from 1 to 3 mm, the total power-generating system mass is increased by about 10%. However, the probability of no catastrophic impacts is increased by orders of magnitude, as shown in Table 5, for all interplanetary missions. It is for this reason that generous armor thicknesses are recommended.

Furthermore, the major armor problem may not necessarily lie in large mass requirements, but rather in the development and fabrication of configurations which result in lightweight elements for component systems of planetary and interplanetary spacecraft. Fabrication

Table 5. Summary of protection requirement ratio \mathcal{R} for planetary and interplanetary missions

Mission	Mission time ^a T , days	Spacecraft terminal mass ^b , lb	Protection requirement ratio, \mathcal{R}	Primary radiator ^c				
				Armor thickness for constant probability, $P_{(0)} = 0.95$		Probability for no failure for various armor thicknesses,		
				Near-Earth Δ_e , cm	Mission Δ_m , cm	Armor thickness, cm		
						0.100	0.200	0.300
Solar probe (to 0.1 AU)	355	14000	0.503	0.198	0.100	0.9509	0.9969	0.9994
Mercury orbit (elliptical)	235	14100	0.566	0.179	0.101	0.9479	0.9967	0.9994
Venus orbit (circular), 1000 km	417	15400	0.779	0.206	0.160	0.7098	0.9791	0.9959
2500 km			0.730		0.150	0.7675	0.9938	0.9968
5000 km			0.496		0.102	0.9456	0.9966	0.9993
Mars orbit (circular), 1000 km	417	15400	0.481	0.206	0.099	0.9520	0.9970	0.9994
2500 km			0.480		0.099	0.9523	0.9970	0.9994
5000 km			0.479		0.099	0.9526	0.9970	0.9994
Asteroid probe (to 5.2 AU)	440	16500	0.516	0.209	0.108	0.9330	0.9957	0.9992
Jupiter orbit (elliptical)	833	15000	0.432	0.245	0.106	0.9378	0.9960	0.9992
Uranus probe	1007	12500	0.435	0.256	0.111	0.9237	0.9951	0.9990
Saturn orbit (elliptical)	1060	12400	0.415	0.260	0.108	0.9330	0.9957	0.9992
Out of ecliptic, 20°	417	15500	0.478	0.206	0.099	0.9528	0.9970	0.9994
30°		13200						
40°		10000						
Neptune probe	1277	15200	0.406	0.272	0.110	0.9264	0.9953	0.9991
Pluto probe	1469	12300	0.397	0.282	0.112	0.9228	0.9951	0.9990
Lunar encounter	80	18100	0.720	0.137	0.099	0.9528	0.9970	0.9994

^aPropulsion time.
^bInitial mass in orbit is 20,000 lb.
^cBased on 31.0 m². Armor material is beryllium.

techniques may require armor thicknesses greater than those specified by the spacecraft system design requirement, resulting in a higher degree of resistance to catastrophic impact damage than necessary.

C. Penetration and Spalling

The results shown in Table 5 for each specified interplanetary mission are based on the penetration resistance of meteoroid impact damage. The \mathcal{R} values shown are directly applicable for estimating the protection requirements for the resistance of spallation. This is accomplished by simply modifying the value of K_1 of Eq. (11) to include the spalling phenomenon. The value of K_1 for flat surfaces is generally suggested to be 2.0. However, consideration should be given to the component's

geometry and material differences. An example is the radiator tube. Its convex liner is enveloped by armor which presents a discontinuity to impact-energy transmission because of the existing interface between the two different materials, thereby reducing the potential damage.

D. Erosion

Abrasive action by cosmic dust particles is most troublesome to optical surfaces and coatings designed for temperature-control requirements (Ref. 15). To find the erosion caused by the expected meteoric hazard for the integrated time exposure for any mission, the erosion rate $(d\psi/dt)_e$ (Ref. 52, 53) for a near-Earth flux environment and the normalized flux-intensity profile $I(t)$ must

be known. The estimated erosion for any defined interplanetary mission may be expressed as

$$\psi = \left(\frac{d\psi}{dt} \right)_e \cdot \left(\int_{t=0}^T I(t) dt \right)_v = \mathcal{R}_v^{\beta} \cdot T_v \cdot \left(\frac{d\psi}{dt} \right)_e \quad (47)$$

The flux-intensity profiles, shown in Fig. 11-20, indicate that the major erosive damage to spacecraft components is most likely to occur during the early phase of mission flight, i.e., the spiral-out to escape phase. The remaining phases of the mission are relatively free from this type of hazard, except for very near planetary orbital

phases. If erosion-sensitive-type surfaces are rated primarily for the heliocentric transfer trajectory, allowance must be made to compensate for the probable erosion during the spiral-out to escape phase.

Zodiacal light measurements, Fig. 4, reveal that the flux intensity of the abrasive dust particles is much more sensitive to geocentric distance than assumed by the meteoroid model. This phenomenon, when considered, would yield smaller \mathcal{R} values than those obtained in this study. However, the values shown in Table 5, when substituted into Eq. (47), will yield conservative results for the erosion magnitude of spacecraft systems during interplanetary and planetary missions.

VI. DISCUSSION

The meteoroid model, defined in Section IIE, suggests that the meteoroid concentration found in interplanetary space located near 1 AU solar distance, and in the ecliptic plane, is 10^{-3} of the concentration found in the near vicinity of the Earth for the damaging-size particles under consideration. Assume that there is one order of magnitude of uncertainty concerning this concentration difference. Suppose, then, a second meteoroid model is constructed and defined as follows: the particle concentration in the same interplanetary space location is 10^{-2} of that found in the near vicinity of the Earth, and the particle concentration in the asteroid region is 10 times as intense as the concentration found in the interplanetary region. Furthermore, suppose that a third meteoroid model is constructed to assign a greater degree of uncertainty to the selected meteoroid model. This third model may be defined as follows: the particle concentration in the interplanetary space near 1 AU solar distance is 10^{-1} of that found in the near vicinity of the Earth, and the particle concentration in the asteroid region is three times as intense as that found in the interplanetary region. The protection requirement ratios \mathcal{R} for a mission may be computed for the latter two model criteria.

The \mathcal{R} values as a function of the different models for three missions are listed in Table 6 for a system probability of no catastrophic impacts $P_{(0)}$ of 0.95. The results in Table 6 show that the change in the \mathcal{R} values is small, relative to appreciable degrees of model uncertainty. This indicates that the meteoric hazard of the interplanetary space environment is not a governing hazard for an interplanetary mission because of the lower concentration of meteoroidal particles found in this region. Data from existing satellites, space probes, and the recent *Mariner 2* spacecraft appear to confirm that the meteoroid hazard in interplanetary space is of a significantly lower order of magnitude than may have been expected.

A spacecraft trajectory out of the plane of the ecliptic is likely to minimize frequent meteoroid impacts for an interplanetary mission, since sporadic meteoric debris is predominately concentrated within 20 deg of the ecliptic plane. For an example, consider a Saturn orbiter mission which has a trajectory inclined greater than 20 deg to the ecliptic plane. The \mathcal{R} value for this mission will decrease only about 0.07% compared to that value found for a mission which has a trajectory in the plane of the

Table 6. Results of protection requirement ratio \mathcal{R} as a function of model uncertainty

Mission	\mathcal{R} values for various meteoroid models		
	Selected model (Section IIE)	Second model ^a	Third model ^a
Venus orbiter (1000 km)	0.779	0.779	0.790
Jupiter orbiter (elliptical)	0.432	0.434	0.483
Saturn probe	0.415	0.417	0.478
^a These models are defined in Section 6.			

ecliptic. It may then be surmised that utilizing a trajectory out of the ecliptic plane to decrease the magnitude of the interplanetary meteoric hazard is not economical, especially when considering the propellant requirement necessary to accomplish an out-of-the-ecliptic trajectory.

The meteoroid model suggests that Venus possesses a large planetary meteoric hazard. However, since there is most likely less meteoric debris inside the solar distance of 1 AU than the meteoroid model suggests, the expected planetary meteoric hazard for both Venus and Mercury missions may be significantly less. Also, planetary meteoric debris may be more sensitive to planetocentric distance as suggested by zodiacal light studies. Thus, the \mathcal{R} values found for these missions (Table 5), which include the planetary meteoric hazard estimated by the model, are considered to be conservative.

The selected values for the parameters K_4 , K_5 , and \bar{H} in the penetration model (Eq. 16) which are employed in

this study, are assumed to be applicable for most spacecraft materials exposed to an impact process. There may be a degree of uncertainty as to the generalized application of these values. However, any error in the \mathcal{R} value resulting from the use of inexact values for these parameters is greatly reduced, since the penetration model is normalized [i.e., Eq. (36)]. Furthermore, because all the variables and parameters are each normalized in this analysis, it is believed that any reliable penetration model, if substituted for the selected penetration model, would yield results very similar to those obtained in this analysis.

Since the meteoroid model assumes that the meteoroid flow direction is isotropic, the armor requirement rating should be based on the nonoccluded vulnerable area of a component regardless of its orientation in space. However, sporadic meteoroids predominately travel in heliocentric orbits near the plane of the ecliptic at small inclinations in interplanetary space. Since the probability of encountering meteoroid impact by sporadic cometary debris is significantly greater than for any other type of meteoric matter, it is reasonable to assume that less damaging impacts are likely to occur if the vulnerable surface is positioned parallel to the ecliptic plane and follows a trajectory of direct motion. Therefore, it is most likely that a flat spacecraft configuration oriented parallel to the ecliptic plane will possess a smaller number of probable catastrophic impacts by sporadic meteoric debris than if the configuration were oriented perpendicular to the ecliptic plane.

VII. CONCLUSION

Armor requirements for the resistance of meteoroid penetration during interplanetary missions are found to be a fraction of that required for a near-Earth orbiter mission due to the expected decrease in meteoric concentration in the space traversed.

This study suggests that the escape-from-Earth phase contributes relatively the greatest hazard of meteoroid impact damage to interplanetary spacecraft for all the selected missions except the low-altitude Venus orbiter. For example, the hazard potentials during the Jupiter orbiter mission are found (Fig. 11) to have the following fractions of the total armor thickness requirement: escape from Earth, 80.64%; interplanetary space, essentially none; asteroid region, 19.20%; planetary orbital phase, 0.12%. Furthermore, the flux intensity decreases with an increased geocentric distance. It is therefore beneficial to deshroud the spacecraft at higher altitudes to minimize the number of probable meteoroid impacts.

Proposed high-power generation systems assume the requirement for higher operating temperature levels pri-

marily to decrease the very massive heat-rejection system. For interplanetary missions this constraint may be relaxed, since armor thicknesses are sufficiently reduced. A tradeoff to a lower heat-rejection temperature may, therefore, be employed to produce a higher cycle efficiency and, consequently, less total heat dissipation. Because protection requirements for interplanetary missions are reduced, either higher probabilities of no catastrophic damage by meteoroid impacts can be achieved, or less massive spacecraft systems can be utilized for the scientific exploration of interplanetary and planetary space.

Errors covering the measurement of meteoroidal characteristics may be minimized by gathering more complete information to which developed statistical procedures may better be applied to describe the many variations and average overall state of meteoric particles. Thus, when better data covering meteoric debris in the regions traversed by exploratory spacecraft are known, their incorporation would enable a refinement of the results of this study.

ACKNOWLEDGMENT

The author expresses his sincere gratefulness to Mr. R. J. Beale for stimulating interest in the meteoroid problem and also for his many helpful comments concerning this Report; to Dr. L. D. Jaffe for his critical review of the paper and for his many valuable comments concerning the nature of meteoroids; to Dr. E. C. Posner for his valuable discussions and help in the development of the analysis; to Mrs. E. W. Speiser and Dr. R. R. Stephenson for providing the interplanetary and planetary trajectories; to certain colleagues of the Advanced Propulsion Engineering Section for their useful comments, which served to increase the clarity of presentation; and to Mrs. M. H. Horton for programming and computing the numerical results.

REFERENCES

1. Watson, F. G., *Between the Planets*, Harvard University Press, Cambridge, Mass., Revised Edition, 1956.
2. Verniani, F., "On the Density of Meteoroids," *Il Nuovo Cimento, Organo Della Societa Italiana Di Fisica*, Vol. 26, No. 2, October 16, 1962.
3. Gallagher, P. B., and V. R. Eshelman, "Sporadic Shower Properties of Very Small Meteors," *Geophysical Journal*, Vol. 65, No. 6, June 1960.
4. Davidson, E. H., and P. C. Winslow, Jr., *Space Debris Hazard Evaluation*, NASA Technical Note D-1105, Lewis Research Center, Cleveland, Ohio, December 1961.
5. Soberman, R. K., *Micrometeorite Collection from a Recoverable Sounding Rocket*, GRD Research Note No. 71, Geophysics Research Directorate, Air Force Cambridge Research Lab., Bedford, Mass., November 1961.
6. Soberman, R. K., and L. Della Lucca, *Micrometeorite Measurements From the Midas II Satellite*, GRD Research Note No. 72, Geophysics Research Directorate, Air Force Cambridge Research Lab., Bedford, Mass., November 1961.
7. Halliday, I., "Diffusion Effects Observed in the Wake Spectrum of a Geminid Meteor," in *Smithsonian Contributions to Astrophysics, Proceedings of the Symposium on the Astronomy and Physics of Meteors*, Smithsonian Astrophysical Observatory, Cambridge, Mass., August 28–September 1, 1961, Vol. 7, Smithsonian Institution, Washington, D.C., 1963, pp. 161–169.
8. Whipple, F. L., "Dust and Meteorites," *Astronautics*, Vol. 7, No. 6, August 1962, pp. 40–42.
9. Gault, D. E., E. M. Shoemaker, and H. J. Moore, *Spray Ejected from the Lunar Surface by Meteoroid Impact*, NASA Technical Note D-1767, National Aeronautics and Space Administration, Washington, D.C., April 1963.
10. Dole, S. H., "The Gravitational Concentration of Particles in Space Near the Earth," in *Planetary Space Science*, Vol. 9, Pergamon Press Ltd., New York (printed in Northern Ireland), 1962, pp. 541–553.
11. Fesenkov, V. G., "On the Density of Meteoric Matter in Interplanetary Space in the Light of the Possible Existence of a Dust Cloud Around the Earth," *Soviet Astronomy*, Vol. 5, No. 6, May–June 1962.
12. Beard, D. B., "Interplanetary Dust Distribution," *The Astrophysical Journal*, Vol. 128, 1959, pp. 496–506.
13. McKinley, D. W. R., *Meteor Science and Engineering*, McGraw-Hill Book Co., Inc., New York, 1961.
14. Hawkins, G. S., "Visual Determination of the Radiant Distribution of Sporadic Matter," *Astronomical Journal*, Vol. 62, No. 1251, Sept. 1957, pp. 234–240.
15. Volkoff, J. J., *Temperature-Control Engineering of Nuclear-Electric Spacecraft*, Technical Report No. 32-232, Jet Propulsion Laboratory, Pasadena, May 15, 1962.
16. Jaffe, L. D., and J. B. Rittenhouse, *Behavior of Materials in Space Environment*, Technical Report No. 32-150, Jet Propulsion Laboratory, Pasadena, March 1961.
17. Kashcheyev, B. L., and K. V. Kostilyov, "Meteor Rates Observed by Radio-Echo Techniques During the IGY-IGC Period," in *Smithsonian Contributions to Astrophysics, Proceedings of the Symposium on the Astronomy and Physics of Meteors*, Smithsonian Astrophysical Observatory, Cambridge, Mass., August 28–September 1, 1961, Vol. 7, Smithsonian Institution, Washington, D.C., 1963, pp. 63–65.
18. Hawkins, G. S., "Variation in the Occurrence Rate of Meteors," *Astronomical Journal*, Vol. 61, No. 1243, November 1956.
19. Whipple, F. L., *On Meteoroids and Penetration*, paper presented at the American Astronautical Society, Interplanetary Conference, Los Angeles, Calif., January 1963.
20. McCracken, C. W., W. M. Alexander, and M. Dubin, "Direct Measurement of Interplanetary Dust Particles in the Vicinity of Earth," *Nature*, Vol. 192, November 4, 1961, pp. 441, 442.
21. Bjork, R. L., "Meteoroid Hazard to Nuclear Spacecraft," *Nucleonics*, Vol. 19, No. 4, April 1961.
22. Hibbs, A. R., "The Distribution of Micrometeoroids Near the Earth," *Journal of Geophysical Research*, Vol. 66, 1961, pp. 371–8.
23. Southworth, R. B., On S. H. Dole's paper "The Gravitational Concentration of Particles in Space Near the Earth," *Planetary Space Science*, Vol. 11, 1963, pp. 499–503.

REFERENCES (Cont'd)

24. Dole, S. H., *Meteoroid Concentration by the Earth's Gravitational Field*, Memorandum No. p-2832, Rand Corp., Santa Monica, Calif.
25. Davidson, J. R., and P. E. Sandorff, *Environmental Problems of Space Flight Structures, II Meteoroid Hazard*, NASA Technical Note D-1493, Langley Research Center, Cleveland, Ohio, January, 1963.
26. Mlodnosky, R. F., V. R. Eshelman, and L. A. Manning, *On the Velocity Distribution of Sporadic Meteors*, Scientific Report No. 5, Stanford Electronics Laboratory, Stanford University, Calif., April 1962.
27. Whipple, F. L., and R. F. Hughes, "On Velocities and Orbits of Meteors, Fireballs, and Meteorites," in *Meteors*, T. R. Kaiser, Ed., Pergamon Press, Ltd., London and New York, 1955, pp. 149-156.
28. Nazarova, T. N., "Preliminary Results Concerning the Investigation of Meteor Material Along the Flight Trajectory of the 'Mars-1' Space Probe," *Space Research*, Vol. 1, No. 1, July-August, 1963, pp. 169-171.
29. Babadjanov, P., "Orbital Elements of Photographic Meteors," in *Smithsonian Contributions to Astrophysics, Proceedings of the Symposium on the Astronomy and Physics of Meteors*, Smithsonian Astrophysical Observatory, Cambridge, Mass., August 28-September 1, 1961, Vol. 7, Smithsonian Institution, Washington, D.C., 1963, pp. 63-65.
30. Southworth, R. B., and G. S. Hawkins, "Statistics of Meteor Streams," in *Smithsonian Contributions to Astrophysics, Proceedings of the Symposium on the Astronomy and Physics of Meteors*, Smithsonian Astrophysical Observatory, Cambridge, Mass., August 28-September 1, 1961, Vol. 7, Smithsonian Institution, Washington, D.C., 1963, pp. 261-285.
31. Black, S. D., "The Space Debris Hazard of Interplanetary Exploration," in *Engineering Problems of Manned Interplanetary Exploration*, AIAA Conference, Palo Alto, Calif., September 30-October 1, 1963, American Institute of Aeronautics and Astronautics, Inc., New York, pp. 119-127.
32. Briggs, R. E., "Steady-State Space Distribution of Meteoric Particles Under the Operation of the Poynting-Robertson Effect," *Astronomical Journal*, Vol. 67, No. 10, December 1962.
33. Newburn, R. L., Jr., "The Exploration of Mercury, the Asteroids, the Major Planets and Their Satellites, and Pluto," in *Advances in Space Science*, Vol. III, Academic Press, New York, Spring, 1960.
34. Hagihara, Y., "Gaps in the Distribution of Asteroids," *Astrophysics*, Vol. 5, No. 6, 1961, pp. 59-67.
35. Middlehurst, B. M., and G. P. Kuiper, *The Moon, Meteorites & Comets*, University of Chicago Press, Vol. IV, 1963.
36. Hawkins, G. S., "The Relation Between Asteroids, Fireballs, and Meteorites," *Astronomical Journal*, Vol. 64, No. 1275, December 1959.
37. Snyder, C., H. R. Anderson, M. Neugebauer, and E. J. Smith, "Interplanetary Physics," in *Proceedings of the NASA-University Conference on the Science of Technology of Space Exploration*, Vol. 1, Chicago, November 1-3, 1962, Office of Scientific and Technical Information, National Aeronautics and Space Administration, Washington, D.C., pp. 163-195.
38. Hawkins, G. S., "Asteroidal Fragments," *Astronomical Journal*, Vol. 65, No. 5, June 1960, pp. 318-322.
39. Vsekhsvyatskii, S. K., "Possible Existence of a Ring of Comets and Meteorites Around Jupiter," *Kiev State University, Astronomicheskii Zhurnal*, Vol. 39, No. 2, March-April, 1962, pp. 290-302.
40. Zotkin, I. T., "On the Ring Encircling Jupiter," *Kiev State University, Astronomicheskii Zhurnal*, Vol. 39, No. 2, March-April 1962, pp. 303-304.
41. Whipple, F. L., "A Comet Model III, The Zodiacal Lights," *Harvard College Observatory, Astrophysical Journal*, Vol. 121, No. 3, May 1955, pp. 750-770.
42. Kuiper, G. P., *The Atmospheres of the Earth and Planets*, University of Chicago Press, 1957 edition.
43. Lovell, A. C. B., *Meteor Astronomy*, Oxford at the Clarendon Press, England, 1954.
44. Rodriguez, D., "Meteoroid Shielding for Space Vehicles," *Aero-Space Engineering*, Vol. 19, No. 19, December 1960.
45. Bjork, R. L., "Meteoroids Versus Space Vehicles," *ARS Journal*, Vol. 31, No. 6, June 1961.

REFERENCES (Cont'd)

46. Herrmann, W., and A. H. Jones, "Correlation of Hypervelocity Impact Data," in *Proceedings of the 5th Symposium on Hypervelocity Impact*, Denver, Colo., October 30–November 1, 1961, sponsored under Contract No. Nonr-(G)-0020-62(X), by U.S. Navy, Army, and Air Force, Vol. 1, Part 2, April 1962, pp. 389–438.
47. Loeffler, I. J., S. Lieblein, and N. Clough, *Meteoroid Protection for Space Radiators*, Paper No. 2543–62, Space Power Systems Conference, September 25–28, 1962, American Rocket Society, New York.
48. Beale, R. J., E. W. Speiser, and R. J. Womack, *The Electric Space Cruiser for High Energy Missions*, Technical Report No. 32-404, Jet Propulsion Laboratory, Pasadena, 1963.
49. Melbourne, W. G., *Interplanetary Trajectories and Payload Capabilities of Advanced Propulsion Vehicles*, Technical Report No. 32-68, Jet Propulsion Laboratory, Pasadena, March 31, 1961.
50. Baker, R. M. L., Jr., and M. W. Makemson, *An Introduction to Astrodynamics*, Academic Press, Inc., (London) Ltd., Berkeley Square House, London W. 1., 1962.
51. Mackay, D. B., *Radiant Heat Transfer from Extended Surfaces in a Space Environment*, Institut Francais des Combustibles et de l'Energie pour la Semaine Internationale Consacree a la Transmission de la Chaleur, Paris, France, 1961.
52. Whipple, F. L., "Meteoritic Erosion in Space," in *Smithsonian Contributions to Astrophysics, Proceedings of the Symposium on the Astronomy and Physics of Meteors*, Smithsonian Astrophysical Observatory, Cambridge, Mass., August 28–September 1, 1961, Vol. 7, Smithsonian Institution, Washington, D.C., 1963, pp. 239–248.
53. Beard, D. B., "Meteoritic Impact," *A.R.S. Journal*, Vol. 31, No. 1, January 1961.
54. Seifert, H. S., Editor, *Space Technology*, John Wiley and Sons, Inc., New York, 1959.